FINAL TECHNICAL REPORT ON NASA GRANT NO. NAGW-3953

"STUDIES OF WESTWARD ELECTROJETS AND FIELD-ALIGNED CURRENTS IN THE MAGNETOTAIL DURING SUBSTORMS: IMPLICATIONS FOR MAGNETIC FIELD MODELS"

Principal Investigator: Harlan E. Spence
Institution: Boston University

OVERVIEW

The research carried out during this grant achieved the scientific goals as set forth in the initial proposal. By way of introduction, this research project was initially awarded by NASA to the Principal Investigator (PI) when he was employed by The Aerospace Corporation; the project also has a co-Principal Investigator, Dr. Ramon Lopez, whose funding was separate. The initial proposal was a three-year effort, the first year of which was completed while the PI was an employee of The Aerospace Corporation. During the last year s(coincident with the start date of the period covered in this report), the PI changed institutional affiliation from The Aerospace Corporation to Boston University (BU). Following the move, the PI continued the work on the overall research effort described herein by establishing a "new", restructured two-year grant at BU whose tasks included those of the remaining two years of the initially proposed study, and which included a no-cost extension. This final report documents primarily those elements not described in previous progress reports.

PROJECT HISTORY/EVOLUTION

To put the results of this effort into perspective, it is first important to provide the project context and history owing to the institutional changes and task restructuring. The main thrusts of the overall proposed effort are to understand the three-dimensional structure of the substorm current wedge, its magnetospheric sources, and the magnetic field geometry throughout the magnetotail during the substorm cycle. Our approach has been one of progress through iterative use of data analysis, modeling, and theory. In the first year of the effort, we focused on three main tasks (principal collaborators are shown parenthetically) : establishing the magnetospheric equatorial projection of the ionospheric electrojets using empirical, static magnetic field models (Dr. Ramon Lopez) ; building an improved, pre-onset magnetic field model of the ring current and near-magnetotail region by appealing to empirical, equilibrium plasma pressure profiles (Dr. Anthony T. Lui, Dr. David P. Stern); and including explicitly the effects of field-aligned currents in magnetic field models in order to assess their importance when mapping ionospheric currents to their magnetospheric source regions (Dr. Eric Donovan, Dr. Ramon Lopez). Several presentations of these multi-faceted efforts were reported at scientific meetings and were completed and published.

TASK TRANSITION

During the final period of the effort, all principal collaborators (as well as the PI) of the outstanding tasks experienced institutional changes (Donovan, Lopez, and Spence) and the associated shifts in priorities and duties. This wholescale reorganization led to logistical problems of focusing jointly on the specific remaining tasks begun in the first year that had originally been anticipated for year two of the effort. We reassessed our positions and decided to focus more tightly on the individual pieces of our study during this final part of the funding cycle with the intent that the conclusion of the outstanding tasks begun in the first year of the effort be continued at a low level and finished during the final year of the grant.

FINAL SUMMARY

This section outlines those tasks undertaken in the final year that contribute integrally to the overarching project goals. First, during the final year, it is important to note that the project benefited greatly with the addition of a Boston University graduate student, Ms. Karen Hirsch. Jointly, we made substantial progress on the development of and improvements to magnetotail magnetic field and plasma models. The ultimate aim of this specific task was to assess critically the utility of such models for mapping low-altitude phenomena into the magnetotail (and vice-versa). The bulk of this effort center ed around the finite-width-magnetotail convection model developed by and described by Spence and Kivelson (*J. Geophys. Res., 98*, 15,487, 1993). This analytic, theoretical model specifies the bulk plasma characteristics of the magnetotail plasma sheet (number density, temperature, pressure) across the full width of the tail from the inner edge of the plasma sheet to lunar distances. Model outputs are specified by boundary conditions of the source particle populations as well as the magnetic and electric field configuration.

During the reporting period, we modified this code such that it can be interfaced with the auroral particle precipitation model developed by Dr. Terry Onsager. Together, our models provide a simple analytic specification of the equatorial distribution of fields and plasma along with their low-altitude consequences. Specifically, we have built a simple, yet powerful tool which allows us to indirectly "map" auroral precipitation signatures (VDIS, inverted-V's, etc.) measured by polar orbiting spacecraft in the ionosphere, to the magnetospheric equatorial plane. The combined models allow us to associate latitudinal gradients measured in the ion energy fluxes at low-altitudes with the large-scale pressure gradients in the equatorial plane. Given this global, quasi-static association, we can then make fairly strong statements regarding the location of discrete features in the context of the global picture. We reported on our initial study at national and international meetings and published the results of our predictions of the low-altitude signatures of the plasma sheet.

In addition, the PI was invited to contribute a publication to the so-called "Great Debate in Space Physics" series that is a feature of EOS. The topic was on the nature of magnetospheric substorms. Specific questions of the when and where a substorm occurs and the connection between the auroral and magnetospheric components were discussed in that paper. This paper therefore was derived exclusively from the research supported by this grant.

PRESENTATIONS AND PUBLICATIONS FROM THE ENTIRE GRANT PERIOD

Refereed Publications:

Lui, A. T. Y., H. E. Spence, and D.P. Stern, Empirical modeling of the quiet time nightside magnetosphere, *J. Geophys. Res.*, *99*, 151, 1994.

Fennell, J., J. Roeder, H. E. Spence, H. Singer, A. Korth, M. Grande, and A. Vampola, CRRES observations of particle flux dropout events, *Adv. Space Res.*, *18*, 217, 1996.

Hirsch, K. L., H. E. Spence, T. G. Onsager, Low altitude signatures of the plasma sheet: model predictions of local time dependence, *J. Geomag. Geoelectr.*, *48*, 887, 1996.

Spence, H. E., The what, where, when, and why of magnetospheric substorm triggers, *EOS Transactions of the Amer. Geophys. Union*, *77*, 81, 1996.

Invited Presentations:

Spence, H. E., Magnetotail convection modeling, invited presentation given at the NASA/GSFC Workshop on Magnetospheric Modeling, Greensbelt, MD, May 1994.

Spence, H. E., Directions toward a synthesis of theoretical magnetotail models, invited presentation given at the NSF/GEM Snowmass '94 Workshop, Snowmass, CO, June 1994.

Spence, H. E., Theoretical problems and observational results on plasma sheet dynamics and mapping, *XXI General Assembly IUGG/IAGA Program and Abstracts*, invited presentation to be given at the XXI General Assembly IUGG/IAGA meeting, Boulder, CO, July, 1995.

Contributed Presentations:

Lopez, R. E., E. F. Donovan, H. E. Spence, S. I. Ohtani, The effects of field-aligned currents on magnetic mapping to the near-Earth magnetosphere: A nightside, substorm case study, *EOS Trans. AGU*, *74*, presented at the 1993 Fall AGU meeting, San Francisco, CA, Dec 1993.

Spence, H. E., J. B. Blake, J. F. Fennell, and H. Koons, Diagnosis of high-altitude spacecraft anomalies: phenomenology and expert system analysis, *EOS Trans. AGU*, *75*, presented at the 1994 Spring AGU meeting, Baltimore, MD, May 1994.

Freisen, L. M., J. B. Blake, J. F. Fennell, and H. E. Spence, Observations of energetic electrons and protons in an elliptical, high altitude, high inclination orbit, *EOS Trans. AGU*, *75*, presented at the 1994 Fall AGU meeting, San Francisco, CA, December 1994.

Spence, H. E., K. L. Hirsch, and T. Onsager, Quasi-static auroral precipitation signatures inferred from magnetotail particle transport models, *EOS Trans. AGU*, *75*, presented at the 1994 Fall AGU meeting, San Francisco, CA, December 1994.

Empirical modeling of the quiet time nightside magnetosphere

A. T. Y. Lui

Applied Physics Laboratory, The Johns Hopkins University, Laurel, Maryland

H. E. Spence

Space and Environment Technology Center, The Aerospace Corporation, Los Angeles, California

D. P. Stern

Laboratory for Extraterrestrial Physics, NASA Goddard Space Flight Center, Greenbelt, Maryland

Empirical modeling of plasma pressure and magnetic field for the quiet time nightside magnetosphere is investigated. Two models are constructed for this study. One model, referred to here as T89R, is basically the magnetic field model of Tsyganenko (1989) but is modified by the addition of an inner eastward ring current at a radial distance of ~3 R_E as suggested by observation. The other is a combination of the T89R model and the long version of the magnetic field model of Tsyganenko (1987) such that the former dominates the magnetic field in the inner magnetosphere, whereas the latter prevails in the distant tail. The distribution of plasma pressure, which is required to balance the magnetic force for each of these two field models, is computed along the tail axis in the midnight meridian. The occurrence of pressure anisotropy in the inner magnetospheric region is also taken into account by determining an empirical fit to the observed plasma pressure anisotropy. This effort is the first attempt to obtain the plasma pressure distribution in force equilibrium with magnetic stresses from an empirical field model with the inclusion of pressure anisotropy. The inclusion of pressure anisotropy alters the plasma pressure by as much as a factor of ~3 in the inner magnetosphere. The deduced plasma pressure profile along the tail axis is found to be in good agreement with the observed quiet time plasma pressure for geocentric distances between ~2 and ~35 R_E.

Introduction

Although the magnetosphere has been studied and surveyed extensively for over 3 decades since the advent of spacecraft, there are still outstanding tasks pertaining to the quiet time magnetosphere. One of these is a quiet time magnetospheric model with specification of the magnetic field configuration and the associated equilibrium plasma pressure distribution. In the quiet time Earth's magnetosphere, the inertial force $\rho dv/dt$ is usually insignificant, and therefore force balance should exist between magnetospheric plasma pressure and electromagnetic forces. An explicit configuration resembling the magnetosphere and satisfying force balance has yet to be devised.

Equilibrium of the magnetosphere has been studied theoretically in the two limiting situations of the inner magnetosphere, where the Earth's dipole field dominates, and the magnetotail, where the field arises mainly from the theta-shape tail current system. The inclusion of the transition region between these two simplified situations has proved difficult [*Voigt and Wolf*, 1988]. In the inner magnetosphere, *Sckopke* [1972] studied equilibrium under the assumption of isotropic plasma pressure in a perturbed dipole field. This type of investigation was recently extended by *Zavriyev and Hasegawa* [1989] and *Cheng* [1992] with the more realistic consideration of anisotropy in plasma pressure as observed [e.g., *Lui and Hamilton*, 1992]. The magnetotail equilibrium has been studied analytically [*Harris*, 1962; *Kan*, 1973] as well as examined by numerical simulation [*Toichi*, 1972; *Birn*, 1989; *Hesse and Birn*, 1992]. Unfortunately, no global three-dimensional equilibrium solutions are known. Present global MHD simulations do not stabilize enough to provide them. Two-dimensional numerical solution, when convection is included, appears to evolve in ways that may preclude a steady state equilibrium [*Erickson and Wolf*, 1980; *Erickson*, 1984; *Hau et al.*, 1989], although this may be merely an artifact of the two-dimensional limitation [*Kivelson and Spence*, 1988].

An alternative approach to obtaining equilibrium configurations is to use data. For example, the magnetic field models of *Tsyganenko* [1987, 1989], which give averaged magnetic field values satisfying the static Maxwell's equations, have been used extensively in relating magnetospheric regions to the ionospheric level and vice versa [*Elphinstone et al.*, 1990; *Stasiewicz*, 1991; *Elphinstone and Hearn*, 1992; *Pulkkinen et al.*, 1992]. However, early models of this type were badly out of force balance [*Walker and Southwood*, 1982]. Particularly pertinent questions related to any empirical magnetic field model are therefore the following:

(1) What is the plasma pressure distribution in force equilibrium with the empirical field model?

(2) How is this plasma pressure distribution compared with actual measurements?

Paper number 93JA02647.
0148-0227/94/93JA-02647$05.00

It is quite evident that the availability of plasma pressure distribution in force balance with the magnetic forces in an empirical field model will further enhance its utilization.

Spence et al. [1987, 1989] and *Kan et al.* [1992] have inverted the earlier magnetic field models [*Tsyganenko and Usmanov*, 1982; *Tsyganenko*, 1987] to obtain the equilibrium plasma pressure along the tail axis at midnight by assuming isotropic or nearly isotropic plasma. The goal of this paper is to extend these previous studies in deriving empirical magnetic field models for the quiet time magnetosphere, with the associated plasma pressure in force equilibrium with the model magnetic field and in good agreement with observations. Two features are incorporated, namely, the presence of an eastward inner ring current and the occurrence of anisotropic plasma pressure. These two features are found to be essential in arriving at a realistic plasma pressure profile. This study treats the simple situation in which the dipole tilt angle is zero, making the configuration symmetric and easy to handle without significantly altering the results.

THE MODIFIED MAGNETIC FIELD MODELS

The magnetic field models of *Tsyganenko* [1987, 1989], hereafter referred to as T87L (long version) and T89, have a number of features that lend themselves to easy applications. The magnetic field in these models is given in an analytical form, with most terms bearing physical insights on the various current systems contributing to the total magnetic field at a given location. The coefficients of these terms are obtained through a least-squares fit to actual measurements and are derived separately for different levels of the *Kp* index to allow for the variability of the magnetic field with geomagnetic activity. Since we consider here the quiet time magnetosphere, the activity level chosen for this study corresponds to the $Kp = 0$ level. Modified versions of these field models form the basis from which magnetic field models are constructed here.

The ring current is dominated by the gradient of plasma pressure. At the inner edge of the ring current, the plasma pressure decreases rapidly inward, producing an eastward flowing ring current in the inner magnetosphere [*Lui and Hamilton*, 1992]. This ring current is featured in neither the T87L nor the T89 model. Although this eastward flowing ring current may not alter the magnetic field to a great extent, as will be demonstrated later, its absence tremendously affects the plasma pressure distribution required to maintain equilibrium with the magnetic forces. Without such an eastward flowing current, the plasma pressure in force equilibrium with the magnetic field will have to increase monotonically inward, as indicated by the earlier work of *Spence et al.* [1989] and *Kan et al.* [1992], and is contrary to the observed plasma pressure distribution. Even though the required volume current density for the eastward ring current is small, the $\mathbf{j} \times \mathbf{B}$ force is significant, since the field strength is high (about inversely proportional to the third power of the geocentric distance) in the inner magnetosphere.

To include the inner ring current in the model, we construct its vector potential using a procedure similar to the one employed in the T89 model to represent the outer ring current, i.e.,

$$A_{IRC} = C_{IRC}\rho S_{IRC}^{-3}, \tag{1}$$

where C_{IRC} is a coefficient controlling the intensity of the inner ring current and

$$S_{IRC} = \sqrt{\rho^2 + (a_{IRC} + \xi_{IRC})^2}, \tag{2}$$

$$\xi_{IRC} = \sqrt{z^2 + (D_0 + \gamma_{IRC} h_{IRC})^2}, \tag{3}$$

$$h_{IRC} = 0.5\left[1 + x\left(x^2 + L_{IRC}^2\right)^{-1/2}\right]. \tag{4}$$

The location of the point in space is given in cylindrical coordinates by (ρ, ϕ, z) and in Cartesian coordinates by (x, y, z). The physical significance of the nonlinear parameters is the same as given for the outer ring current by *Tsyganenko* [1989]. The radial scale length a_{IRC} relates to the geocentric distance for the inner ring current. The half thickness of the inner ring current region is represented by D_0. The variation of this thickness with local time, i.e., the difference between dayside and nightside, is controlled by the function h_{IRC} with its scale length L_{IRC}. We find that the flow reversal of the ring current from westward to eastward inside $L \approx 3.5$ can be reproduced reasonably well by adopting the following values for the above parameters: $C_{IRC} = 760$ nT, $a_{IRC} = 1.5\ R_E$, $D_0 = 1.8\ R_E$, $\gamma_{IRC} = -0.2723$ (same as the value for the quiet time outer ring current), and $L_{IRC} = 1.5\ R_E$. To keep the total magnetic moment of the ring currents the same as the original ring current in the T89 model, we have modified the outer ring current strength by

$$C_{RRC} = C_{ORC} - C_{IRC} \times (a_{IRC}/a_{ORC})^2, \tag{5}$$

where the subscripts RRC and ORC denote, respectively, the revised and original outer ring current parameters in T89. It turns out that the modification is extremely slight (only ~0.2%). This model with the inner eastward ring current and a correspondingly modified outer ring current strength is identified hereafter as T89R.

Since the T89 and T89R field models give rather weak magnetic fields in the magnetotail [*Stern and Tsyganenko*, 1992; *Rostoker and Skone*, 1993; *Peredo et al.*, 1993], we have also explored the T87L field model. To take advantage of the fact that the T89R model is better than the T87L model in the inner magnetospheric region, but the reverse is true for the distant tail [*Tsyganenko*, 1989; *Donovan et al.*, 1992], we combine the two field models by constructing a hybrid field model (designated hereafter as TH) with a transition parameter ϵ such that

$$B_{z,TH} = \epsilon B_{z,87L} + (1-\epsilon) B_{z,89R}, \tag{6}$$

$$\epsilon = 0.5 - 0.5 \sin\left(\left(2(x - x_L)/(x_U - x_L) - 1\right)\pi/2\right), \tag{7}$$

where B_z is the z component of the magnetic field along the midnight meridian and subscripts 87L and 89R denote parameters from the T87L and T89R models, respectively. The parameters x_L and x_U are the lower and upper bounds of x for the transition. The transition parameter ϵ is 0 at $x = x_U$ and 1 at $x = x_L$, with a smooth derivative $d\epsilon/dx$ at the end points. The boundary points adopted here are x_U

$= -5\ R_E$ and $x_L = -25\ R_E$. We note that the region of interest in this paper is the equatorial plane along the tail axis in which the magnetic field has only the z component (for a dipole tilt angle of 0°). The divergence of the magnetic field along the tail axis therefore reduces to $\partial B_z / \partial z$. It is clear then that the linear combination of the magnetic fields from the T87L and T89R models as expressed in (6) is also divergence free along the tail axis. On the other hand, if this hybrid model were to be extended beyond the tail axis, there would be a small nonzero divergence if the other field components were not modified accordingly.

Figure 1*a* shows the profiles of magnetic field values in logarithmic scale from the four magnetic field models, i.e., T87L, T89, T89R, and TH, at the equatorial region along the midnight meridian. Note that the four magnetic field profiles are quite different between $x \approx -8\ R_E$ and $-30\ R_E$. The highest magnetic field values come from T87L, followed by TH, T89, and T89R. Although the inclusion of the inner ring current only slightly weakens the magnetic field, this effect is manifested quite dramatically in the extremely low field region of the T89 model, where the field magnitude goes below 1 nT.

The volume current densities from these four models at the equatorial region along the midnight meridian are examined in Figure 1*b*. The T87L model typically gives the lowest current densities among these models. Tailward of $x \approx -10\ R_E$, the T89 and T89R models give almost the same values, whereas the TH model shows noticeably lower current densities between $x \approx -10$ and $-30\ R_E$. The lower values from the TH model, in comparison with the T89 and T89R models, are expected from the influence of the T87L model. Earthward of $x \approx -10\ R_E$, although the current densities from the T89R and TH models are almost identical, those from the T89 and T87L models have different values. Earthward of $x \approx -8\ R_E$, both the T89 and T87L models show a persistent westward current. In contrast, the T89R and TH models show a reversal of westward ring current to an eastward ring current at $-3.5\ R_E$. The presence of this current reversal is modeled to represent the reversal noted from the CCE observations [*Lui and Hamilton*, 1992]. In comparison, we find the observed current densities appear to be higher than the model values at the current density peak but smaller than the model values at distances further downstream. In addition, the observed current densities are more variable, reflecting the filamentary nature of current much like the magnetotail current [*McComas et al.*, 1986].

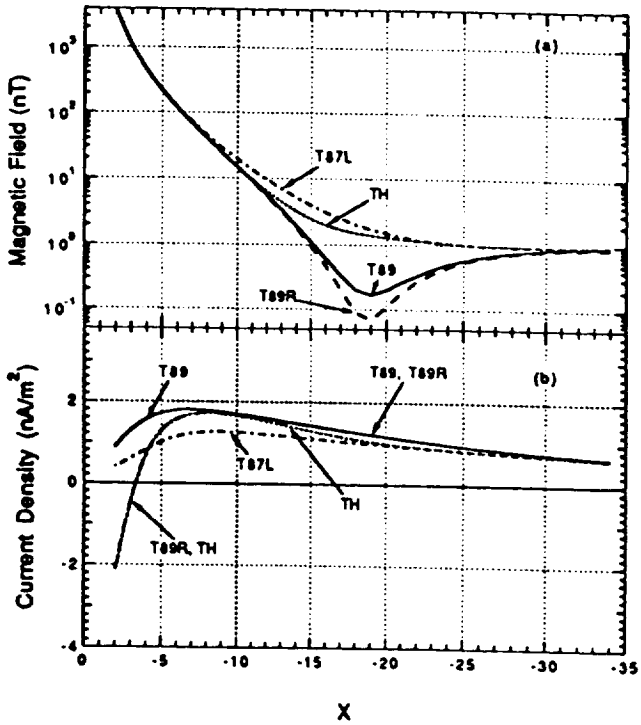

Fig. 1. (*a*) Magnetic field profiles along the midnight meridian at the equatorial plane from four magnetic field models. (*b*) Current density profiles along the midnight meridian at the equatorial plane from four magnetic field models.

The observed anisotropy of plasma pressure taken from *Lui and Hamilton* [1992] is shown in Figure 2 together with an empirical fit. The anisotropy is seen to be large in the inner region and decreases rather systematically at distances further downstream. The empirical fit to the anisotropy is a fifth-order polynomial function of x^{-1}, i.e.,

$$P_\perp / P_\parallel - 1 = a_0 + a_1 x^{-1} + a_2 x^{-2} + a_3 x^{-3} + a_4 x^{-4} + a_5 x^{-5}, \quad (8)$$

with coefficients $a_0 = -0.410554$, $a_1 = -9.94369$, $a_2 = -86.9877$, $a_3 = -504.066$, $a_4 = -1110.73$, and $a_5 = -847.912$. The range of validity for this fit is $-2.5\ R_E > x > -15\ R_E$ such that the plasma pressure is isotropic at $x \approx -15\ R_E$. That the pressure should be isotropic downstream of $x \approx -15\ R_E$ is indicated by the studies of *Stiles et al.* [1978] and *Baumjohann and Paschmann* [1989].

Given a magnetic field model, it is straightforward to compute the magnetic force $\mathbf{j} \times \mathbf{B}$ and determine the pressure force required to balance it. The radial profile of perpendicular plasma pressure can be obtained by integrating

$$\frac{\partial P_\perp}{\partial r} = \left[\mathbf{j} \times \mathbf{B} + (P_\perp - P_\parallel)(\mathbf{b} \cdot \nabla)\mathbf{b}\right]_r, \quad (9)$$

where the subscript r indicates the radial component of the vector quantity, $\mathbf{b}$ is the unit magnetic field vector $\mathbf{B}$, $\mathbf{j}$ is the volume current density, and $P_\perp$ and $P_\parallel$ are the plasma pressure components perpendicular and parallel to the observed magnetic field direction, respectively.

Figure 3*a* shows the result from this computation for the T89R model with the plasma pressure at $x = -34\ R_E$ taken to be 0.074 nPa. This initial value of plasma pressure is obtained by computing the plasma pressure re-

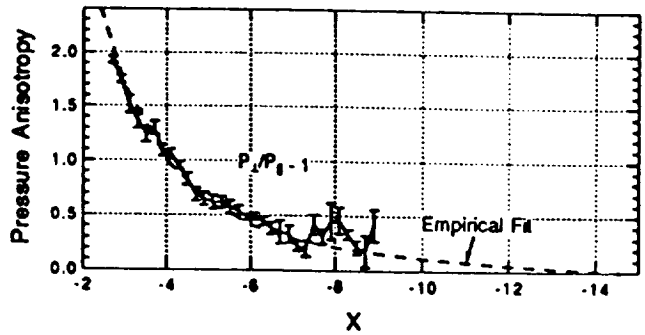

Fig. 2. Observed pressure anisotropy profile of the nightside magnetosphere and an empirical fit.

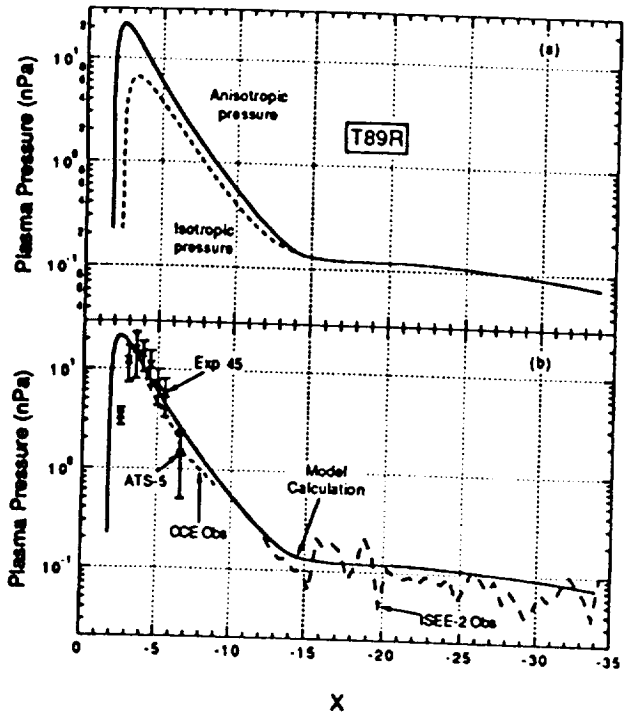

Fig. 3. (*a*) Equatorial profiles of the perpendicular plasma pressure along the midnight meridian inverted from the T89R magnetic field model assuming isotropic plasma pressure (dashed trace) and adopting the pressure anisotropy shown in Figure 2 (solid trace). (*b*) Equatorial profile of the perpendicular plasma pressure along the midnight meridian inverted from the T89R magnetic field model in comparison with measured values of perpendicular plasma pressure from several satellites.

quired at the neutral sheet ($z = 0$) to balance the "asymptotic" magnetic field value for the tail lobe region of the T89R model at that distance. The "asymptotic" magnetic field value is the x component of the field at $z = 20\ R_E$, which in this case is ~13.6 nT. It is worth noting that since the plasma pressure is shown in logarithmic scale, a larger initial value for the plasma pressure will not affect the plasma pressure in the inner magnetosphere significantly. The plasma pressure is assumed isotropic at $x = -15\ R_E$ and further downstream. The computed profile of the perpendicular plasma pressure is given by the solid trace. For comparison, the profile of plasma pressure, assuming pressure isotropy at all distances, is given by the dashed trace. It is quite apparent that the assumption of isotropic pressure results in an underestimate of the plasma pressure at the inner magnetosphere by as much as a factor of ~3. This finding can readily be understood by noting that the plasma pressure anisotropy inside $x \approx -15\ R_E$ for the quiet time magnetosphere is in the sense of $P_\perp > P_\parallel$. With this sense of pressure anisotropy, the second term on the right of equation (9) adds to the first one, thus requiring a larger pressure gradient for force equilibrium, as pointed out earlier by *Lui and Hamilton* [1992].

The computed perpendicular plasma pressure profile is compared with observations from Explorer 45, ATS 5, ISEE 2, and CCE in Figure 3*b*. The ISEE 2 data are taken from *Spence et al.* [1989] for the $Kp = -1$ condition, the CCE data from *Lui and Hamilton* [1992], the ATS-5 data from *DeForest and McIlwain* [1971], and the Explorer 45 data from *Spence et al.* [1989], using measurements of 1- to 872-keV protons presented by *Smith and Hoffman* [1973]. The range of pressure values from Explorer 45 data indicated by the error bars actually spans the observed pressure taken during geomagnetically quiet to disturbed conditions, and thus the lower limit should be used for comparison with the model calculation. As can be seen from Figure 3*b*, the model pressure profile is in general above the observed pressure profile, especially in the outer region. This finding is understandable and is to be expected because the observed pressure is not necessarily obtained right at the equatorial plane and thus is expected to underrepresent the actual observed pressure at the equatorial plane. Inside 4 R_E, the pressure determined from Explorer 45 is noticeably lower than that from CCE values and the model calculation. This difference may be due to the upper energy threshold being only 872 keV for Explorer 45 measurements, whereas that of CCE extends to >4 MeV. It is possible that a significant contribution to plasma pressure inside 4 R_E comes from particles above the 872-keV level. We have evaluated this possibility using several midnight passes of CCE during quiet conditions. We found the ions with energy of >872 keV contributing typically ~50-65% to the plasma pressure at geocentric distances inside 4 R_E. Since the disparity in the determination of pressure between Explorer 45 and CCE is about a factor of 6, we conclude that the different energy passbands can account for a significant portion, but not the entirety, of the observed pressure difference.

Overall, we find very good agreement exists between the observed and computed profiles of plasma pressure on the basis of the T89R model. Another notable feature of the model pressure profile is its relative constancy between the downstream distances of 16 and 25 R_E. This finding indicates the small magnitude of the $\mathbf{j} \times \mathbf{B}$ force in this region. Reexamining Figure 1 reveals that the main reason for the decrease in the $\mathbf{j} \times \mathbf{B}$ force in the T89R model is the small value of the magnetic field in that region (Figure 1*a*), since the volume current density is still substantial at those distances (Figure 1*b*). The more abrupt change in the radial profile of plasma pressure occurs in the downstream distances between $x \approx -12\ R_E$ and $x \approx -15\ R_E$, as noted earlier by *Spence et al.* [1989]. The $\mathbf{j} \times \mathbf{B}$ force is therefore relatively large at the transition region between the dipolelike and taillike field configurations. It is interesting to note that this region may correspond to the hinging point of the tail, where the tangential stress acted on the magnetotail by the solar wind at the tail magnetopause is balanced by the attractive force between the Earth's dipole and the tail current system [*Siscoe and Cummings*, 1969].

A similar plasma pressure profile can be obtained from the TH model, as shown in Figures 4*a* and 4*b*. The plasma pressure based on the formula from *Spence and Kivelson* [1993],

$$P(\text{nPa}) = 89e^{-0.59|x|} + 8.9\,|x|^{-1.53} \qquad (10)$$

is also shown for comparison; the downstream distance x is in Earth radii. The assumption of isotropic pressure gives an underestimate of plasma pressure by as much as a factor of ~3 in the inner magnetosphere as before. The most significant difference between the two anisotropic pressure profiles in Figures 3 and 4 lies in the downstream

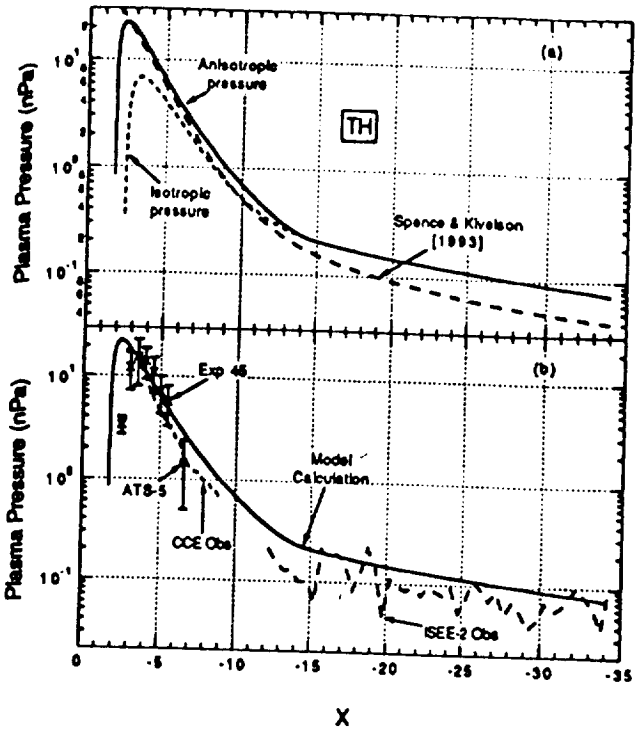

Fig. 4. (*a*) Similar to Figure 3*a* except that the perpendicular plasma pressure is inverted from the TH magnetic field model instead. (*b*) Similar to Figure 3*b* except that the perpendicular plasma pressure is inverted from the TH magnetic field model instead.

region of $x \approx -10$ to -20 R_E. Whereas the T89R profile shows a relatively constant pressure in this region, the other profile shows a continuous pressure increase toward the Earth. This continuous rise, however, only contributes rather insignificantly to the plasma pressure earthward of $x \approx -8$ R_E. The continuous change in plasma pressure reflects a more gradual transition between the dipolelike and taillike field configurations as well as a more x-dependent pressure for the near-Earth tail region in this model than that in the T89R model. The empirical formula by *Spence and Kivelson* [1993] also compares reasonably well with the model profile. The formula gives a good fit to the plasma pressure within the range of $x \approx -2.5$ to -15 R_E but overestimates it inside this region and underestimates it further tailward.

Summary and Discussion

We have investigated two empirical models for the specification of magnetic field and the plasma pressure for the quiet time nightside magnetosphere. The derived magnetic field models are extensions of the previous magnetic field models of *Tsyganenko* [1987, 1989] by the addition of an inner eastward ring current. Furthermore, in constructing the equilibrium plasma pressure along the tail axis in the midnight meridian, we have taken into account the presence of plasma pressure anisotropy in the inner magnetosphere earthward of $x \approx -15$ R_E. An empirical fit to the observed pressure anisotropy in the inner magnetosphere (between 2.5 and 15 R_E) is also provided. These two new features profoundly affect the deduced plasma pressure profile. The first feature leads to an earthward reduction of the plasma pressure in the innermost part of the magnetosphere (geocentric distances of < -3 R_E) as observed. The second feature leads to an appropriate evaluation of the plasma pressure gradient. Without the consideration of plasma pressure anisotropy, the deduced plasma pressure may be underestimated by as much as a factor of ~3. The derived perpendicular plasma pressure is found to be in good agreement with the observed values from ISEE 2, CCE, ATS 5, and Explorer 45. The T89R and TH models therefore provide quite realistic representations along the tail axis in the midnight meridian of not only the quiet time magnetic field but also the associated equilibrium plasma pressure distributions needed to provide the force balance with the magnetic forces in these models. The range of validity for the T89R and TH models in representing the magnetic field, the volume current density, and the anisotropic plasma pressure considered here is -2.5 $R_E > x > -35$ R_E. The present result also supports the earlier findings from *Spence et al.* [1989] that the gradient of plasma pressure shows a relatively large change in the transition region between dipolelike and taillike field configurations.

A region called the inner edge of the plasma sheet has been introduced in the early studies of the energetic particle environment in the magnetosphere [*Vasyliunas*, 1968; *Frank*, 1971]. It is a region characterized by an exponential decrease of electron energy density with decreasing radial distance and is generally located at geocentric distances of ~6 to 8 R_E in the nightside. Many researchers implicitly assume that the inner edge of the plasma sheet is associated with an earthward decrease of the total plasma pressure, and theories on the closure of the large-scale region 2 field-aligned current system [*Iijima and Potemra*, 1978] have been built upon this assumption (see, for example, the review by *Mauk and Zanetti* [1987]). As pointed out by *Mauk and Zanetti* [1987], the observed plasma pressure shows a persistent earthward increase rather than a decrease in the geocentric distances usually ascribed to the inner edge of the plasma sheet. In terms of total plasma pressure, there is no edge at those distances. The plasma commonly identified as constituting the plasma sheet in the outer magnetosphere (tailward of the geocentric distance of ~10 R_E) gradually becomes the hot ring current particle population. The absence of a large-scale plasma pressure decrease in the so-called inner edge of the plasma sheet indicates the necessity to modify the conventional mechanism for closing the large-scale region 2 field-aligned current. An alternative means for the region 2 field-aligned current closure in an earthward increasing plasma pressure condition has been proposed by *Lui and Hamilton* [1992]. They have suggested, based on the work of *Sato and Iijima* [1979], that the correct sense of field-aligned current will be generated if the $\nabla P_\perp$ vector is inclined toward the midnight meridian more than the ∇B vector in both the premidnight and the postmidnight sectors, since the sense of the field-aligned current is determined by the sign of the triple product of B, $\nabla P_\perp$, and ∇B. Figure 5 illustrates this configuration graphically. In other words, a plasma pressure in the midnight sector slightly enhanced over that of the adjacent local time sectors will satisfy the requirement.

At least two aspects of this study can be improved in the future. One is to extend the calculation to other local times besides midnight, and the second is to extend it in the z direction to cover the region away from the equato-

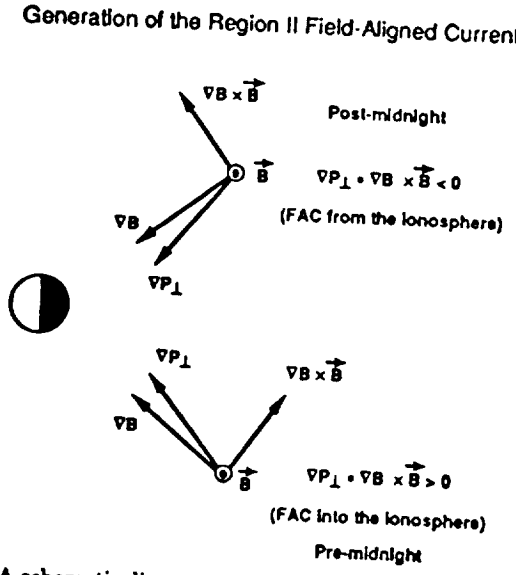

Fig. 5. A schematic diagram to illustrate the relative orientation of the vectors ∇B and $\nabla P_\perp$ to give the correct sense of the field-aligned current system for region 2.

rial plane. The former extension requires a better assessment of the variation of pressure anisotropy as a function of local time, which is not presently available. The latter extension requires integrating the variations of both the perpendicular and parallel components of the plasma pressure in a plane. If these extensions were to be incorporated in the TH model, one must also address the extension of the divergence-free property of the magnetic field along the tail axis to other regions in the magnetosphere, which can be accomplished by considering a linear combination of the vector potentials of the T87L and T89R models instead of their magnetic fields. These improvements will be the subject of a future investigation.

Acknowledgments. We would like to thank N. A. Tsyganenko for providing his earlier magnetic field models on which the new models are built. This work was supported by the Atmospheric Sciences Section of the National Science Foundation (Grant ATM-9114316 to the Johns Hopkins University Applied Physics Laboratory). The work at The Aerospace Corporation was supported by the Space Physics Program of the National Aeronautics and Space Administration under Grant NAGW-3353.

The Editor thanks T. Pulkkinen and R. H. Comfort for their assistance in evaluating this paper.

REFERENCES

Baumjohann, W., and G. Paschmann, Determination of the polytropic index in the plasma sheet, *Geophys. Res. Lett.*, *16*, 295, 1989.

Birn, J., Three-dimensional equilibria for the extended magnetotail and the generation of field-aligned current sheets, *J. Geophys. Res.*, *94*, 252, 1989.

Cheng, C. Z., Magnetospheric equilibrium with anisotropic pressure, *J. Geophys. Res.*, *97*, 1497, 1992.

Donovan, E. F., G. Rostoker, and C. Y. Huang, Region of negative B_z in the Tsyganenko 1989 model neutral sheet, *J. Geophys. Res.*, *97*, 8697, 1992.

Elphinstone, R. D., and D. J. Hearn, Mapping of the auroral distribution during quiet times and substorm recovery, *Eur. Space Agency Spec. Publ., ESA SP 335*, 13, 1992.

Elphinstone, R. D., K. Jankowska, J. S. Murphree, and L. L. Cogger, The configuration of the auroral distribution for interplanetary magnetic field B_z northward, 1, IMF B_z and B_y dependencies as observed by the Viking satellite, *J. Geophys. Res.*, *95*, 5791, 1990.

Erickson, G. M., On the cause of X-line formation in the near-Earth plasma sheet: Results of adiabatic convection of plasma sheet, in *Magnetic Reconnection in Space and Laboratory Plasmas, Geophys. Monogr. Ser.*, vol. 30, edited by E. W. Hones, Jr., p. 296, AGU, Washington, D.C., 1984.

Erickson, G. M., and R. A. Wolf, Is steady state convection possible in the Earth's magnetosphere?, *Geophys. Res. Lett.*, *7*, 897, 1980.

Frank, L. A., Relationship of the plasma sheet, ring current, trapped boundary, and plasmapause near the magnetic equator and local midnight, *J. Geophys. Res.*, *76*, 2265, 1971.

Harris, E. G., On a plasma sheath separating regions of oppositely directed magnetic field, *Nuovo Cimento*, *23*, 116, 1962.

Hau, L. N., R. A. Wolf, G. H. Voigt, and C. C. Wu, Steady state magnetic field configurations for the Earth's magnetotail, *J. Geophys. Res.*, *94*, 1303, 1989.

Hesse, M., and J. Birn, Three-dimensional MHD modeling of magnetotail dynamics for different polytropic indices, *J. Geophys. Res.*, *97*, 3965, 1992.

Kan, J. R., On the structure of the tail current sheet, *J. Geophys. Res.*, *78*, 3773, 1973.

Kan, J. R., W. Sun, and W. Baumjohann, A hybrid equation of state for the quasi-static central plasma sheet, *Geophys. Res. Lett.*, *19*, 421, 1992.

Iijima, T., and T. A. Potemra, Large-scale characteristics of field-aligned currents associated with substorms, *J. Geophys. Res.*, *83*, 599, 1978.

Kivelson, M. G., and H. E. Spence, On the possibility of quasi-static convection in the quiet magnetotail, *Geophys. Res. Lett.*, *15*, 1541, 1988.

Lui, A. T. Y., and D. C. Hamilton, Radial profiles of quiet time magnetospheric parameters, *J. Geophys. Res.*, *97*, 19,325, 1992.

Mauk, B. H., and L. J. Zanetti, Magnetospheric electric fields and currents, *Rev. Geophys.*, *25*, 541, 1987.

McComas, D. J., C. T. Russell, R. C. Elphic, and S. J. Bame, The near-Earth cross-tail current sheet: Detailed ISEE 1 and 2 case studies, *J. Geophys. Res.*, *91*, 4287, 1986.

Peredo, M., D. P. Stern, and N. A. Tsyganenko, Are existing magnetospheric models excessively stretched?, *J. Geophys. Res.*, *98*, 15,343, 1993.

Pulkkinen, T. I., R. J. Pellinen, H. E. J. Koskinen, H. J. Opgenoorth, J. S. Murphree, V. Petrov, A. Zaitzev, and E. Friis-Christensen, Auroral signatures of substorm recovery phase: A case study, in *Magnetospheric Substorms, Geophys. Monogr. Ser.*, vol. 64, edited by J. R. Kan, et al., p. 333, AGU, Washington, D.C., 1992.

Rostoker, G., and S. Skone, Magnetic flux mapping considerations in the auroral oval and the Earth's magnetotail, *J. Geophys. Res.*, *98*, 1377, 1993.

Sato, T., and T. Iijima, Primary sources of large-scale Birkeland currents, *Space Sci. Rev.*, *24*, 347, 1979.

Sckopke, N., A study of self-consistent ring current models, *Cosmic Electrodynamics*, *3*, 330, 1972.

Siscoe, G. L., and W. D. Cummings, On the cause of geomagnetic bays, *Planet. Space Sci.*, *17*, 1795, 1969.

Smith, P. H., and R. A. Hoffman, Ring current particle distributions during the magnetic storms of December 16-18, 1971, *J. Geophys. Res.*, *78*, 4731, 1973.

Spence, H. E., and M. G. Kivelson, Contributions of the low-latitude boundary layer to the finite width magnetotail convection model, *J. Geophys. Res.*, *98*, 15,847, 1993.

Spence, H. E., M. G. Kivelson, and R. J. Walker, Static magnetic field models consistent with nearly isotropic plasma pressure, *Geophys. Res. Lett.*, *14*, 872, 1987.

Spence, H. E., M. G. Kivelson, R. J. Walker, and D. J. McComas, Magnetospheric plasma pressures in the midnight meridian: Observations from 2.5 to 35 R_E, *J. Geophys. Res.*, *94*, 5264, 1989.

Stasiewicz, Polar cusp topology and position as a function of interplanetary magnetic field and magnetic activity: Comparison of a model with Viking and other observations, *J. Geophys. Res.*, *96*, 15,789, 1991.

Stern, D. P., and N. A. Tsyganenko, Uses and limitations of the Tsyganenko field models, *Eos Trans. AGU*, *73*, 489, 1992.

Stiles, G. S., E. W. Hones, S. J. Bame, and J. R. Asbridge, Plasma sheet pressure anisotropies, *J. Geophys. Res.*, *83*, 3166, 1978.

Toichi, T., Two-dimensional equilibrium solution of the plasma sheet and its application to the structure of the tail magnetosphere, *Cosmic Electrodynamics*, *3*, 81, 1972.

Tsyganenko, N. A., Global quantitative models of the geomagnetic field in the cislunar magnetosphere for difference disturbance levels, *Planet. Space Sci.*, *35*, 1347, 1987.

Tsyganenko, N. A., A magnetospheric magnetic field model with a warped tail current sheet, *Planet. Space Sci.*, *37*, 5, 1989.

Tsyganenko, N. A., and A. V. Usmanov, Determination of the magnetospheric current system parameters and development of experimental geomagnetic field models based on data from IMP and HEOS satellites, *Planet. Space Sci.*, *30*, 985, 1982.

Voigt, G.-H., and R. A. Wolf, Quasi-static magnetospheric MHD processes and the "ground state" of the magnetosphere, *Rev. Geophys.*, *26*, 823, 1988.

Walker, R. J., and D. J. Southwood, Momentum balance and flux conservation in model magnetospheric magnetic fields, *J. Geophys. Res.*, *87*, 7460, 1982.

Vasyliunas, V. M., A survey of low-energy electrons in the evening sector of the magnetosphere with Ogo 1 and Ogo 3, *J. Geophys. Res.*, *73*, 2839, 1968.

Zavriyev, A., and A. Hasegawa, The equilibrium dayside magnetosphere, *J. Geophys. Res.*, *94*, 10,039, 1989.

A. T. Y. Lui, Applied Physics Laboratory, The Johns Hopkins University, Johns Hopkins Road, Laurel, MD 20723.

H. E. Spence, Space and Environment Technology Center, The Aerospace Corporation, Los Angeles, CA 90045.

D. P. Stern, Laboratory for Extraterrestrial Physics, NASA Goddard Space Flight Center, Greenbelt, MD 20771.

(Received April 15, 1993;
revised July 12, 1993;
accepted September 3, 1993.)

Pergamon

Adv Space Res Vol. 18, No. 8, pp. (8)217–(8)228, 1996

0273-1177/96 $9.50 + 0.00

0273-1177(95)00991-4

CRRES OBSERVATIONS OF PARTICLE FLUX DROPOUT EVENTS

J. Fennell,[1] J. Roeder,[1] H. Spence,[2] H. Singer,[3] A. Korth,[4] M. Grande[5] and A. Vampola[6]

[1] *The Aerospace Corporation, P.O. Box 92957, Los Angeles, CA 90009, U.S.A.*
[2] *Boston University, Boston, MA 02215, U.S.A.*
[3] *NOAA R/E/SE, Boulder, CO 80303, U.S.A.*
[4] *Max Planck Institute for Aeronomy, Lindau, Germany*
[5] *Rutherford Appleton National Laboratory, Chilton, Didcot, Oxfordshire, U.K.*
[6] *P.O. Box 10225, Torrance, CA 90505, U.S.A.*

ABSTRACT

The complete disappearance of energetic electrons was observed by CRRES in the near geosynchronous region in 7.5% of the orbits examined. These total flux dropouts were defined by the fluxes rapidly dropping to levels below the sensitivity of the MEA energetic electron spectrometer on the CRRES satellite. They were separated into those that were only energetic electron dropouts and those that were associated with energetic ion and plasma dropouts. Approximately 20% of the events showed dropouts of all particle fluxes, and these were usually coincident with large increases in the local magnetic intensity and signatures of strong current systems. The energetic particle instruments and magnetometer on CRRES provide a detailed picture of the particle and field responses to these unusual conditions. Both the local morning and dusk events were associated with strong azimuthal (eastward) and radial changes in the magnetic field indicative of a strong current system approaching and sometimes crossing the CRRES position at the time of the flux dropouts. The direction of the field changes and the details of particle observations are consistent with CRRES passing through the plasma sheet boundary layer and entering the tail lobe for a significant number of the events.

INTRODUCTION

Changes in the energetic particle distributions at near geosynchronous altitudes are often observed in association with substorm processes and the large scale boundary motions that often accompany them /1/. For example, on the dayside, the compression of the magnetosphere by solar wind pressure pulses can move the magnetopause inside the geostationary orbit /2,3/. This is evidenced by the "dropout" of energetic particle fluxes observed by spacecraft in the dayside magnetosphere /2,3,4/. This occurs because the interplanetary energetic particle fluxes are orders of magnitude lower than those found inside the magnetosphere. Thus, when the boundary is "pushed" earthwards of a magnetospheric satellite's orbital position, it changes from observing high magnetospheric fluxes to observing the low interplanetary flux in a very short time (i.e., the flux drops out). It is relatively uncommon to observe such magnetopause crossing events near geosynchronous orbit /2/. In the nightside magnetosphere, the distortion of the geomagnetic field caused by the intensified cross-tail currents which arise during the substorm growth phase can cause significant modification in the energetic particle angular distributions and intensities. These can become so extreme as to cause complete flux dropouts of the energetic particles (see for example refs. /5/ and /6/). Normally, such signatures are observed in the midnight sector, and often the fluxes only decrease drastically but do not totally drop out. If magnetospheric satellites enter the tail lobe, which does not contain significant fluxes of energetic particles under normal conditions, the energetic particles would "drop out". Normally, near-earth satellites, such as those with orbits that do not extend beyond geosynchronous altitudes, do not enter the tail lobes. Often the post-dropout recovery of the energetic particle fluxes are associated with the expansion onset of a substorm /5/. It is relatively uncommon to observe strong energetic particle flux dropouts in the dawn and dusk sectors /1/. Korth et al. /7/ has recently reported the occurrence of energetic particle dropouts in the local morning sector and Moldwin et al. /8/ have

observed flux dropouts at nearly all local times and tail lobe entry by geosynchronous satellites from dusk to dawn in the nightside magnetosphere. In this paper we use data similar to that of Korth et al. /7/ but extend the study to include all local times reached by CRRES (Combined Release and Radiation Effects Satellite). By using the local magnetic field and particle data in combination we can show the relationship between the particle dropouts and the active current systems at the time of such events.

INSTRUMENTATION

The CRRES satellite was launched on 25 July 1990 into an elliptical orbit with a geocentric perigee of ~6720 km, apogee of ~39950 km and an inclination of 18.15°. /9/ The initial local time of apogee was ~8.7 MLT, and after 1072 orbits (near end of life 14 October 1991) it was at ~14 MLT. The orbital inclination in combination with its ~9.6 hour orbital period and the Earth's tilted magnetic dipole allowed CRRES to reach L shells up to and somewhat beyond L=8 on a regular basis. The CRRES near apogee altitude coverage has some gaps in local time. These are the local time intervals near noon on the dayside (from ~09 through 13 MLT) and in the early post-midnight region near 01 MLT. The post-midnight coverage gap resulted from the suspension of instrument operations during the CRRES near-apogee eclipse periods.

The instruments used for this study are primarily the Medium Electrons A (MEA) Spectrometer /10/, the Magnetosphere Ion Composition Sensor (MICS) /11/, and the CRRES magnetometer /12/. We have also examined some EPAS (Electron and Proton Wide-Angle Spectrometer) data /13/ and the LEPA (Low Energy Plasma Analyzer) data /14,15/ to determine whether a plasma signature was present or not. The MEA measures electrons from ~153 keV to 1.5 MeV in 17 differential energy channels /10/, while the MICS measures ions from ~1.2 to 426 keV/charge with ion charge and mass composition over mass dependent energy ranges /11/. The MEA and MICS sensors are mounted perpendicular to the CRRES spin axis, which is sun pointed at all times, and cover a relatively wide range of particle pitch angles during a spin period (~30 sec). The EPAS sensor covers the energy ranges of 21 - 285 keV and 37 - 3200 keV for electrons and ions, respectively /13/. EPAS has multiple fields of view (FOV) and, by combining the data from the multiple FOV, basically obtains a complete pitch angle distribution every spin period. The LEPA also has multiple FOV and provides complete pitch angle coverage of electrons and ions with energies of 0.12 to 28 keV/q. In the LEPA summary data referenced here /15/, only the precipitating and perpendicular plasma electron and ion fluxes were available.

OBSERVATIONS

For this study we required that the one-minute spin-averaged MEA fluxes, at all energies $\gtrsim$ 153 keV, drop to background levels. This is a rather stringent requirement and basically deletes most of the growth-phase-only signatures /5/ from the study. The MEA criteria were selected because of the easy access to the data and the large geometric factor and good sensitivity of this instrument (see Table 1). The total MEA flux dropout to background levels was chosen to eliminate the more usual flux decreases that occur commonly in the magnetosphere near geosynchronous altitudes. A total of 117 flux dropout events met this requirement between CRRES orbits 76 and 1065 (from 26 August 1990 through 11 October 1991). There were as many as five separate flux dropouts observed in a single orbit. In total, the 117 dropouts were distributed over 70 orbits, as shown in Table 2.

The 117 events were further reduced to those which showed a dropout of the energetic ions ($\gtrsim$20 keV). Only 53 events satisfied this criterion. Finally, we selected only those events which showed a dropout of the plasma ions and plasma electrons, respectively, as shown in Table 2. From the initial selection of 117 events, only 20 showed a dropout of all particle fluxes.

Flux dropouts were observed to occur at all local times on the nightside magnetosphere. (We specifically eliminated obvious cases of magnetopause crossings from this study.) The most unexpected regions for them to occur are the local morning and local evening. In these regions the magnetic field topology is usually fairly dipole-like for L shells below 7. Thus, we expect that the

distorted magnetic configurations that lead to flux dropouts should be rarely observed there by CRRES, even at the moderate latitudes it attains. Also, one would naively expect that the local morning and local evening occurrences should show similar features. We present below one case each of local evening and local morning flux dropouts as examples of the phenomena observed by CRRES before we discuss the statistics of the dropouts. It should be noted that CRRES was in the northern hemisphere near local morning apogee and in the southern hemisphere near local evening apogee.

TABLE 1. Instrument Parameters

	Geometric Factor	Minimum Measurable Flux
MEA	2.14 - 5.88 cm^2 sr keV [ref. /10/]	~ 3 x 10^{-3} Electrons/(cm^2 sec sr keV)
MICS	4.4 x 10^{-3} cm^2 sr keV [ref. /11/]	~ 23 Ions/(cm^2 sec sr keV)
LEPA	--	~ 5 x 10^4 particles/(cm^2 sr) at 0.12 keV [estimated from summary spectrograms]

TABLE 2. Particle Flux Dropout Statistics

	Number of		Kp Value			|Dst| Value		
	Dropouts	Orbits	< 3	3 - 6	> 6	< 30	30 - 100	> 100
Energetic Electrons	117	70	17	65	35	34	46	37
Energetic Ions	53	34	6	27	20	13	21	19
Plasma Ions	33	20	0	20	13	5	15	13
Plasma Electrons	23	14	0	17	6	4	10	9
All Particles	20	14	0	15	5	4	10	6

Number of orbits examined = 944

Local Evening Flux Dropout

An example of an event which showed the dropout of all particle fluxes on the local evening side of the magnetosphere is presented in Figures 1 and 2. Figure 1 shows the energetic electron data from MEA for this event, which occurred during CRRES orbit 767 on 5 June 1991. The flux from several different electron energies are shown on the plot, with the highest trace being that of the ~ 153 keV electrons. The decreasing flux levels correspond to increasing energy. The bold trace represents the response of a "background" monitor (BKG) within the MEA. The ~153 keV electron fluxes were required to drop to or below the BKG level before they were identified as a total flux dropout. There were three such periods of total electron flux dropout identified in Figure 1: one near 1500 UT at L=7.0, 17.8 MLT and -21.8° magnetic latitude (MLAT), the second near 1600 UT at L=7.4, 18.5 MLT and MLAT = -21.6°, and the third near 1850 UT at L=6.0, 20.7 MLT and MLAT = -18.5°.

The lower panels of Figure 2 show energy-time spectrograms of several channels of MICS data for the same orbit. DCR is a measure of the total ion flux independent of species and thus is similar to the measurement made by a total ion plasma instrument such as the LEPA, only at somewhat higher energies (~ 7 - 400 keV/q versus 0.12 - 28 keV/q). The MICS "≥ Alpha" channel represents the total flux of all ions with mass ≥ 4 AMU. The other channels measure the fluxes of the H^+, He^+, He^{++} and O^+ above a mass dependent energy threshold /11/. There are periods in the MICS data where essentially all ions dropped out, especially during the 1600 UT event. Note that each O^+ spectrum has been averaged over 8 minutes, which means there were a few counts in each interval that straddles

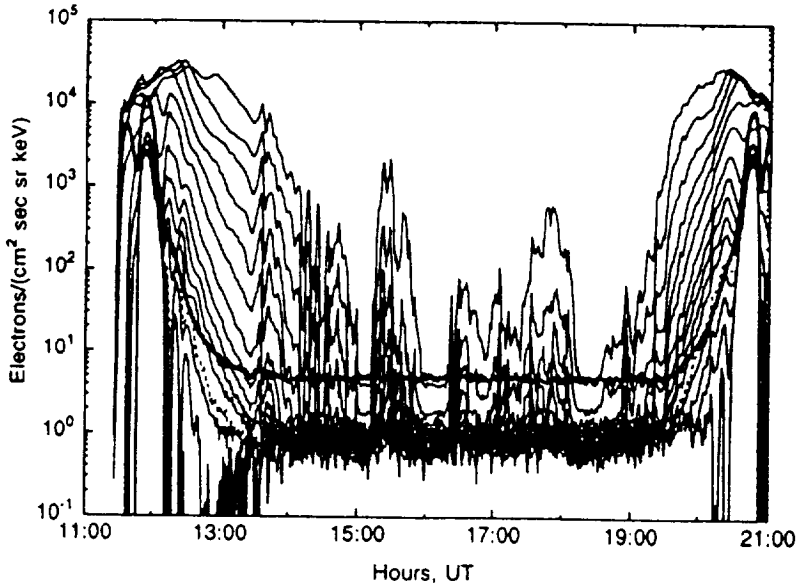

Fig. 1. Energetic electron fluxes from the CRRES MEA sensor during orbit 767 on 5 June 1991. The topmost trace is the flux of ~153 keV electrons and the succeeding traces are for successively higher energies /9/. The bold line represents the response to a background monitor (**BKG**). The ~153 keV electron fluxes were required to be at or below **BKG** in order to qualify as a flux dropout for this study. For this period, the energetic electron flux dropouts occurred at 54100, 57600 and 67800 sec (or 1500, 1600 and 1850 UT).

the flux dropout's edges. It should be noted that the He^+ flux dropped well before the rest of the ions and that it recovered later than the other ions too. This relationship between the two charge states of Helium was often observed in the flux dropout events. This would be expected if He^{++} is presumed to be the dominant He ion in the outer magnetosphere, as is expected for a solar wind source in which He^+ is generated via charge exchange from He^{++}. The He^+ would be most prevalent on the lower L shells deep inside the plasma sheet. If the flux dropout were the result of a reconfiguration of the magnetosphere that caused the CRRES satellite to be on field lines that thread the distant tail near the interface between the plasma sheet and tail lobe field lines, then the ion composition just prior to and just after the flux dropout should reflect that of the distant plasma sheet, as was apparently the case for this event.

The upper three panels of Figure 2 show the magnetometer measurements for this event. The data are presented as the differences between the Tsyganenko 1987 field model /16/ for Kp = 3 and the observed values. The direction ($\hat{b}$) was taken as the Tsyganenko field direction. The reference coordinate directions $\hat{b}$, $\hat{r}$ and $\hat{w}$ are in the directions parallel to the Tsyganenko field, earthward in the plane containing $\hat{b}$ and the radius vector from the center of the earth to CRRES and westwards, respectively, as shown in Figure 3.

∂Bb, ∂Br and ∂Bw are the differences (residuals) between the measured and the Tsyganenko model field. As can be seen by the magnitudes of these components, especially ∂Br, the magnetic field intensity at CRRES was stronger than normal and very "tail-like". There was also a significant, but varying, westward component. The large ∂B_r and ∂B_w indicate that strong currents were flowing in the neighborhood of CRRES. Specifically, near the onsets of the particle dropouts, the field became more tail-like and rotated from a westward to an eastward direction. At each flux recovery the field became less tail-like (although still much more tail-like than normal) and rotated back towards the meridian plane (where ∂Bw = 0). In particular, a strong dipolarization occurred in conjunction with the ion flux recovery near 1515 UT. A second (momentary) and third dipolarization occurred near 1620 UT, where there was first a short ion flux recovery with subsequent dropout followed by a permanent ion flux recovery near 1628 UT (see DCR in Figure 2 near 15200-1530 UT). These field

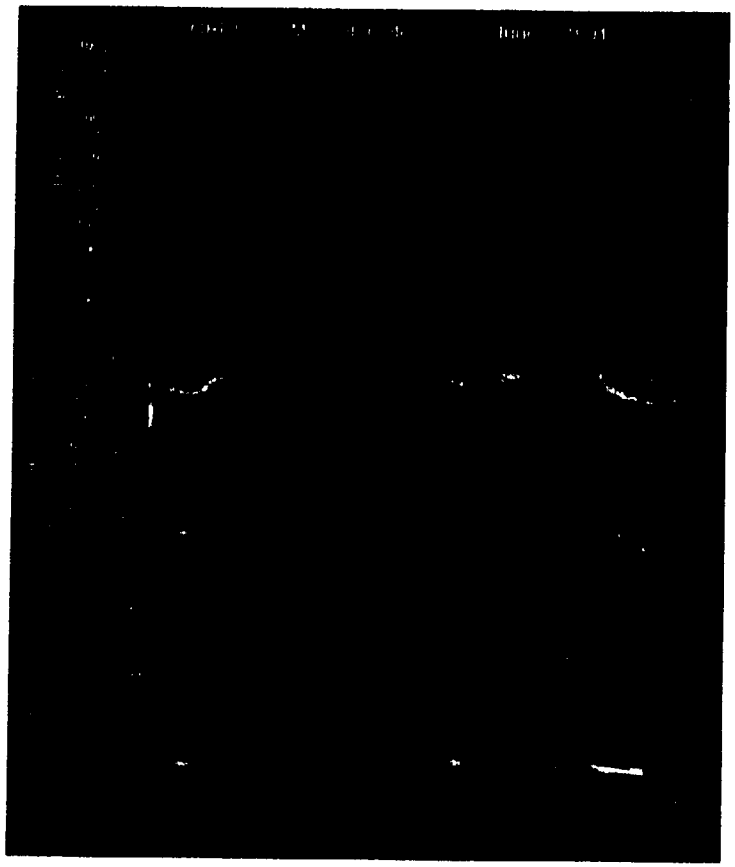

Fig. 2. CRRES magnetometer and MICS data for 11-21 UT on 5 June 1991 (orbit 767). Top three panels show the deviations of the three components of the magnetic field from the Tsyganenko model /16/. The bottom six panels show energy-time spectrograms of different ion species measured by the MICS instrument (see text).

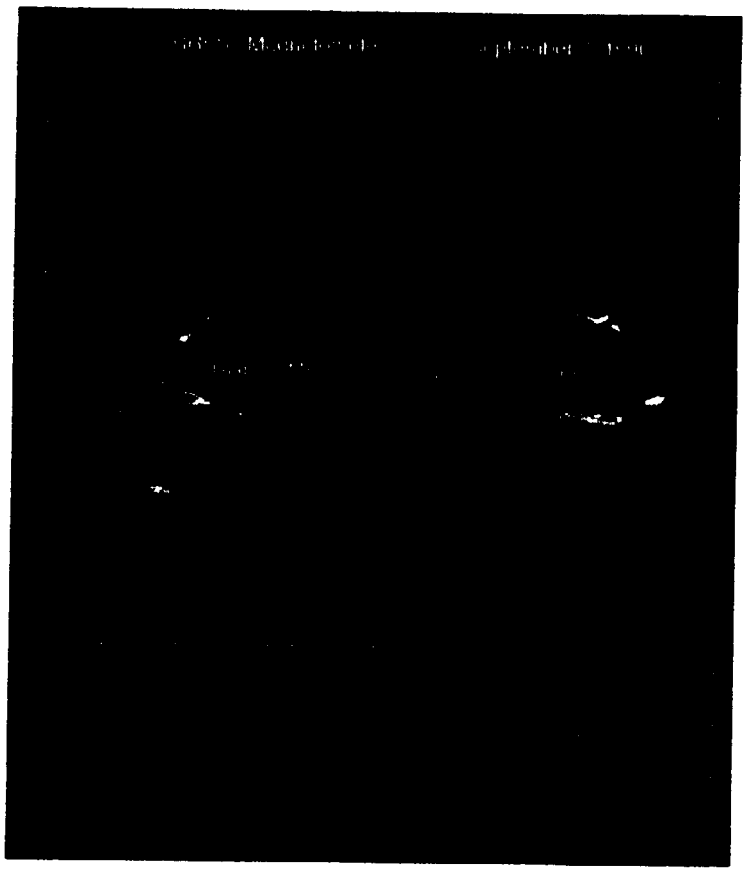

Fig. 5. Like Figure 2 except 09-19 UT on 7 September 1990 (orbit 106). Top three panels show the deviations of the three components of the magnetic field from the Tsyganenko model /16/. The bottom five panels show energy-time spectrograms of different ion species measured by the MICS instrument (see text).

signatures are consistent with the CRRES satellite having been approached and crossed by a Region 1 current system as the particle fluxes dropped out and then recovered.

While there was a total energetic electron flux dropout near 1850 UT, there was not a comparable dropout in the energetic ion fluxes. The intensification of the ion fluxes near 1700 UT (61200 sec) occurred simultaneously with a weak energetic electron recovery. The ion fluxes returned to lower levels by 1730 UT, which is just prior to the electron flux recovery that peaks near 1752 UT.

The plasma data (not displayed here) showed a total plasma electron dropout in conjunction with both of the energetic ion dropouts in Figure 2. The plasma ions also dropped out but only just prior to the energetic particle flux recoveries near 1515 UT and 1625-1628 UT. Both the plasma electrons and ions showed the same momentary flux recovery, subsequent short dropout and final recovery during this latter period, as was observed in the energetic ions (ref. Figure 2). Like the energetic ions, the plasma data did not show a flux dropout near 1850 UT and indicated that CRRES remained in a hot plasma sheet plasma. The only other significant feature in the plasma data was the occurrence of low energy (< 1 keV) field-aligned electron fluxes just prior to and immediately after the plasma and energetic particle dropouts discussed above.

Local Morning Flux Dropout

Figure 4 shows an example of energetic electron total flux dropouts observed by CRRES near local morning on 7 September 1990. There were five flux dropout intervals (marked by shaded vertical bars in Figure 4) which started near 1300, 1308, 1320, 1332 and 1409 UT. We have plotted the CRRES magnetic difference data (as discussed above) on the same plot for comparison. Note that the ∂Br was positive when the magnetic field had tail-like conditions because CRRES was in the northern hemisphere, whereas ∂Br was negative during the local evening tail-like conditions discussed above.

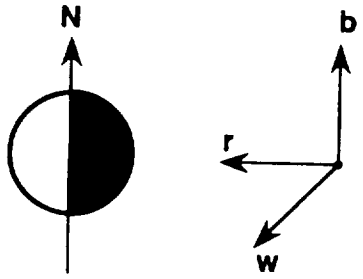

Fig. 3. Coordinate system used for detrended magnetic field data. $\hat{b}$ is parallel to the Tsyganenko field vector, $\hat{r}$ is earthward in the plane defined by $\hat{b}$ and the radius vector from the center of the earth to CRRES and $\hat{w}$ is westward.

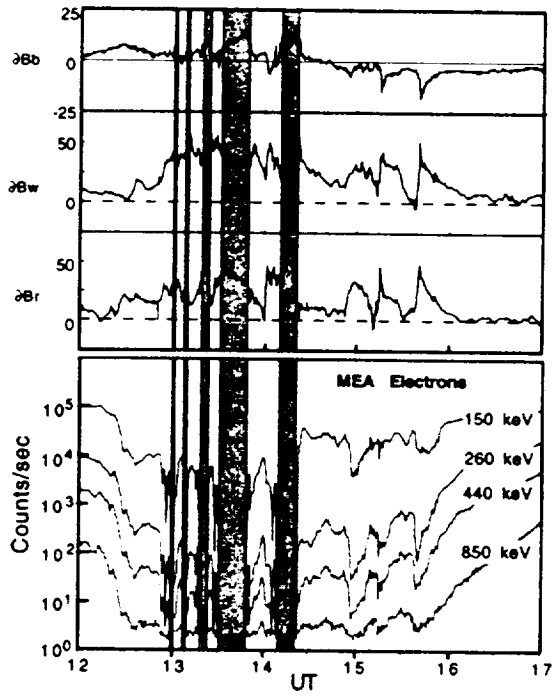

Fig. 4. Energetic electrons and detrended magnetic field data for 7 September 1990 (CRRES orbit 106). The flux dropout onsets are 1300, 1308, 1320, 1332 and 1409 UT.

In both cases, the ∂Bw turned from westward towards zero or eastward at the flux dropout onsets and returned westward at the flux recovery. Like the local evening observations, the field is compressed (positive ∂Bb) during the dropouts. Also, the field was tail-like at the dropout onset and dipolarized at the flux recovery. These signatures, like those of the local evening dropouts, are consistent with CRRES having been approached and crossed by a region 1 current system at the flux dropout and at recovery. This would be consistent with CRRES having entered the tail lobe on the local morning side of the magnetosphere.

Figure 5 shows the MICS energetic ion data and, again, the magnetic field difference plots for this event. In this case, there was a one-to-one correspondence between the energetic electron flux dropouts and the energetic ion flux dropouts. The primary difference between Figure 5 and Figure 2 was the relative absence of O+ ions throughout the magnetosphere on 7 September . Other than this lack of O^+ and He^{++} ions on 7 September, flux dropout features were remarkably identical for these two events that were observed on opposite sides of the magnetosphere.

Examination of the plasma data (not shown here) showed that there was a one-to-one correspondence between the energetic particle flux dropouts and the plasma dropouts for the 7 September events. The narrow dropouts at 1300 and 1308 UT were barely resolved in the summary plasma electron plots and somewhat less clear in the ion plots. Like the local evening case, intense low energy field-aligned electron fluxes were observed just prior to and immediately after the flux dropouts. In general, such field-aligned "soft" electron fluxes were observed near the majority of the energetic ion flux dropouts and at nearly all of the plasma dropouts.

Flux Dropout Statistics

As mentioned above, we examined the energetic ion, magnetic field and plasma data that were available for all 117 energetic flux dropout events. Table 2 summarizes the breakdown into the different categories according to whether the energetic ions and plasma showed flux dropouts and some crude ranges of K_P and D_{ST} levels for the corresponding events. In general, the K_P values observed at the time of the flux dropouts were moderate to high. This is presented graphically in Figure 6, where the distributions of both energetic electron and energetic ion flux dropouts in K_P and D_{ST} are shown.The dominance of moderate to high K_P values indicates the flux dropouts occur during disturbed periods, as would be expected for the strong currents observed in association with the dropouts (e.g., see Figures 2 and 5). But, there is no strong dependence on D_{ST} The majority of the flux dropouts occurred during relatively low or modest D_{ST} This is somewhat surprising. It indicates that magnetic storm conditions are not necessary for the flux dropouts to occur. One might have expected that flux dropouts would have been more prevalent during the magnetically disturbed conditions generally associated with larger ring current enhancements.

Figures 7 and 8 show the distribution of the CRRES flux dropouts in magnetic local time and L and in magnetic latitude and L, respectively. Note that the paucity of events in two different local time regions, one post-midnight (0 - 2 MLT) and one near noon (9-14 MLT), partially reflects the lack of coverage in these regions. [CRRES apogee never reached the near noon sector and the instruments were turned off in the post-midnight sector during the eclipse season.] There was only one obvious magnetopause crossing observed by CRRES and this was eliminated from the data set. The different panels in Figures 7 and 8 correspond to the distribution of energetic electron dropouts (a), the energetic ion dropouts (b) and the plasma ion dropouts (c), respectively. Note that when one required that the plasma ions disappear to have a total particle dropout, there remained only two events that met this criterion on the morning side but a significant number on the evening side. All flux dropout events were observed at magnetic latitudes 10° or more above and below the magnetic equator. The preponderance of the dropouts occurred for $L > 6.6$ and all but two occurred for $L > 5.5$. This indicates that to have a good probability of observing particle dropouts requires a satellite to be at or above geosynchronous altitude and/or at moderate to high magnetic latitudes.

The trend of the points in Figure 8 to move to higher latitude with larger L shell is a result of the CRRES orbital configuration. As noted in the introduction, CRRES only reached $L \leq 6.3$ at the

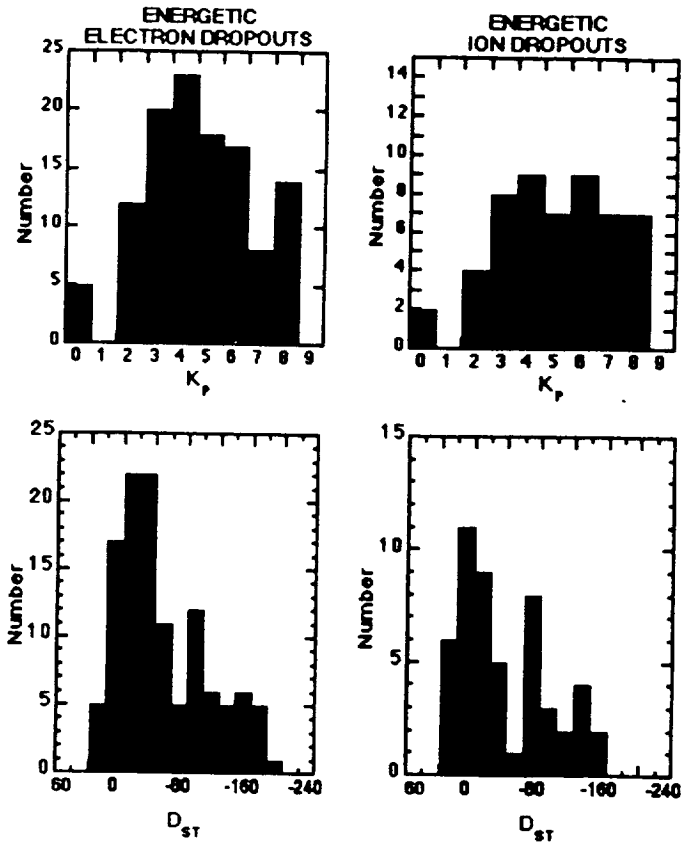

Fig. 6. Energetic ion and electron dropout occurrence frequency versus Kp and D_{ST}.

magnetic equator, but because of its moderate 18° inclination it could reach higher L shells when apogee was off the magnetic equator. The ~10 hour orbital period allowed the CRRES apogee to pass through a significant range of magnetic latitudes on a weekly basis. The morning side data were taken in the late summer and fall of 1990 while the midnight to dusk data were taken in the spring through summer of 1991. The combination of Figures 7 and 8 show that the morning side events all occurred in the northern hemisphere and the midnight through dusk events occurred in the southern hemisphere.

Finally, we looked at the changes in the local magnetic field at the times of the total plasma dropout onsets to see if they were all consistent with the picture, described above, of the CRRES satellite crossing (or being crossed by) a Region 1 current system, entering the tail lobes and then returning at flux recovery. We grouped the events into morning side and dusk side local time regimes, as shown in Table 3. We examined in detail the pre- and post-dropout field trends and the changes that occurred at flux dropout onset and recovery. We categorized the changes, as shown in Table 3, according to whether the field was tail-like (had a significant radial component) or was becoming tail-like at onset and whether the azimuthal component changed and in which direction. In all cases, the field was either strongly tail-like or became tail-like at flux dropout onset. In the majority of cases, the azimuthal component turned eastward at onset. Since all the morning side events occurred in the northern hemisphere and the dusk side events were in the southern hemisphere, an eastward rotation of the field would be consistent with crossing a Region 1 current system in the respective local time sectors. So it is clear from Table 3 that the majority of total plasma dropout events occurred as the CRRES satellite crossed (or was crossed by) the boundary between the plasma sheet and tail lobe as evidenced by the passage of the Region 1 current system along with the strongly tail-like field geometry and the loss of all particle fluxes.

TABLE 3. Field Changes During Total Plasma Dropout Onsets

	∂Bw			∂Br			
MLT	Eastward	Westward	No Change	More Tail Like	Less Tail Like	No** Change	Number of Events
3 - 9	5	1	--	4	--	2	6
15 - 21	11	1	1	10	--	3	13

** ∂Br remained large but constant

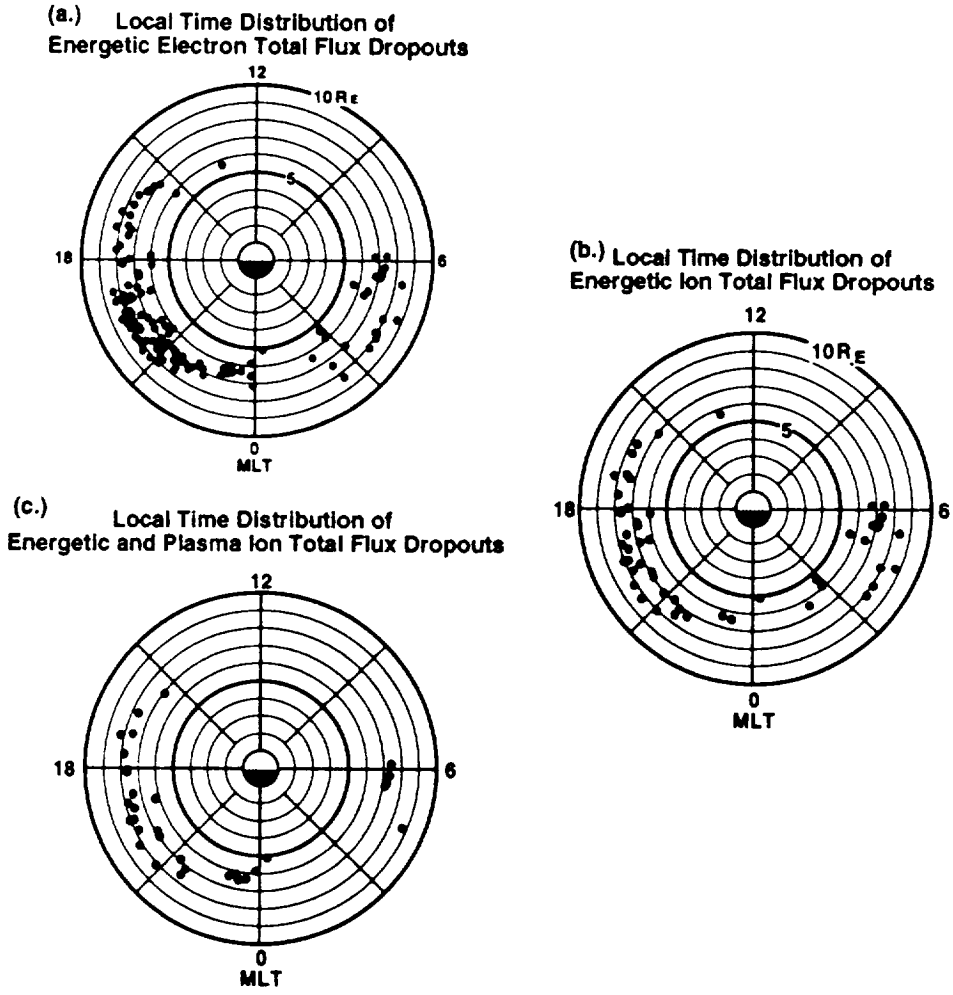

Fig. 7. Distribution of flux dropouts in magnetic local time and L shell: (a) for engergetic electrons, (b) for energetic ions, and (c) for plasma ions.

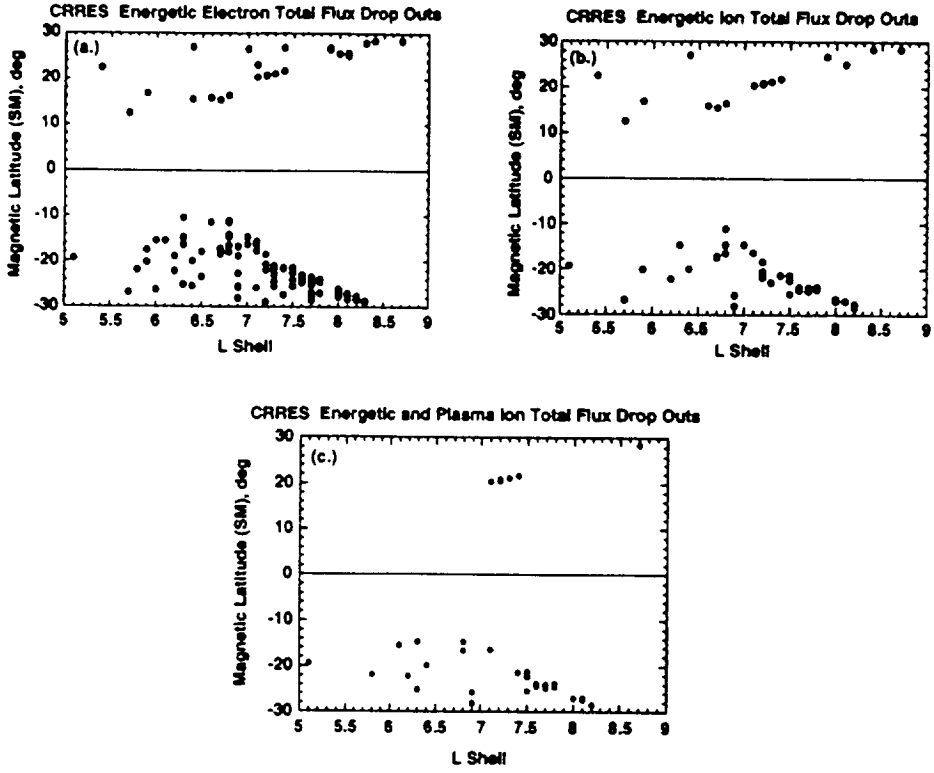

Fig. 8. Distribution of flux dropouts in magnetic latitude and L shell: (a) for energetic electrons, (b) for energetic ions, and (c) for plasma ions.

SUMMARY AND CONCLUSIONS

The local morning and local evening flux dropout events described here and the total plasma dropouts represented in Table 3 clearly show that CRRES entered the magnetotail lobe during these flux dropouts. In general, as seen in the two events shown, the recovery from the flux dropouts was not associated with a signature of substorm expansion onset at CRRES. Given that most of the events were observed away from the midnight sector, it is possible that the substorm signature was not observable by CRRES. To determine whether there was a substorm associated with these events requires examining ground magnetometer and other satellite data, which is beyond the scope of the present work, but will be done as part of a continuing effort on this subject (see Korth et al. /7/).

We emphasize that care was taken to eliminate magnetopause crossings (only one found) from this data set by examining the plasma data for signatures of magnetosheath plasma. In all cases, very significant currents were flowing near the CRRES satellite as evidenced by the strong changes in the magnetic field topology from average conditions. The field was generally tail-like, indicating that the satellite was near the inner edge of the cross-tail current system. The actual current system configuration that can give rise to such strongly tail-like conditions as were observed near 5.5-6.5 MLT (see Figure 5) and 17.8-19.0 MLT (see Figure 2) is not clear, and its details require more observational constraints than are provided by a single satellite measurement.

It should be noted that the majority of the energetic particle flux dropouts included in this data set had rapid onsets like those shown in Figures 1, 2, 4 and 5. The criterion that the lowest energy channel from the CRRES MEA sensor must drop to background levels removed most of the events that had slowly decreasing growth-phase-like flux decrease signatures /5/. While this reduced the total

number of electron flux dropout candidates, it provided a list of those most likely to also show energetic ion and plasma dropouts. The high sensitivity of both the energetic electron and ion sensors (MEA and MICS, see Table 1) allowed us to set very stringent minimum flux levels for our dropout identifications. As can been seen in Figures 1, 2, 4 and 5, these thresholds were orders of magnitude below typical magnetospheric levels and comparable to the cosmic ray background response of the sensors. It should also be noted that all particle data in this study were averaged over one or more satellite rotations so that details of the particle angular distributions were not visible.

The difference between the number of energetic electron and energetic ion flux dropouts is most likely a result of the ions greater gyro-radii. That is, the ions are observable within an ion gyro-radius of the plasma-sheet/tail-lobe boundary on the tail lobe side of the boundary, which is much deeper in the tail lobe than an energetic electron can reach. In a follow-on study we will examine the energetic ions and electrons in greater detail and use the available angular distribution data /13/ to "sound" the boundary in the neighborhood of the flux dropout intervals. This should help to more clearly delineate the differences between the energetic electrons and ions during the flux dropout events. It is most likely that, in some cases, the satellite approached to within a particle gyro-radius of the boundary but did not pass through it.

The local time and seasonal results described above are in apparent disagreement with the recent results of Moldwin et al. for events observed at geosynchronous orbit, wherein they found a preference for the southern hemisphere dropouts to occur during the winter season and the northern hemisphere dropouts to occur during the summer season /8/. In our case, the season did not appear to matter. But, the Moldwin et al. results were from data taken near the geographic equator, whereas the CRRES orbit sampled a much wider range of geographic and geomagnetic latitudes. Therefore, CRRES observed the dropouts only when it was more than 10° away from the geomagnetic equator. We did not note the geographic position of the dropouts during this study. This will be done during the expanded study noted above.

At this point we do not know whether the field-aligned plasma electrons, observed at the edges of the flux dropouts, are moving towards or away from the earth since the actual direction is not indicated in the summary data. This will be examined in greater detail in a later paper. It is important because it will more clearly identify the plasma regime that CRRES was immersed in just prior to the flux dropouts and at the recovery. Given the strong field-aligned currents detected by the magnetometer in these regions, it is possible these intense electrons may be the current carrying particles.

It is clear from the above discussion that much remains to be done on the subject of flux dropouts. Some of the questions that arise are: How can the field be so tail-like at dusk and dawn on such low L shells (≤ 7)? Why are the electron dropouts more prevalent than ion dropouts? What are the motions of the tail-lobe boundary relative to CRRES at the times of the dropouts? What is the configuration of the tail-lobe boundary and the corresponding current systems during such events? Were the solar wind conditions extreme (i.e., was the magnetosphere compressed)? Were substorm onsets associated with many of the events? Were such flux dropout events observable at other spacecraft, such as those in geosynchronous orbit. The answer to these and other questions will be the focus of our future work on this subject.

ACKNOWLEDGMENTS

We would like to thank D. Hardy, K. Kerns and the U. S. Air Force Phillips Laboratory/GPSP for producing the LEPA data and N. Watkins and A. Johnstone for making it available for this study. We would also like to thank G. Reeves, M. Thomsen and M. Moldwin for useful discussions on the topic of flux dropouts. The EPAS and MICS instruments were designed and constructed with support from the Max-Planck-Gesellschaft zur Förderung der Wisenschaften. The MEA instrument and the MEA, MICS and EPAS digital data processors were designed and constructed at The Aerospace Corporation. The work performed at The Aerospace Corporation was supported in part by the U.S. Air Force System Command's Space System Division under contract No. F04701-91-C-0089.

REFERENCES

1. Walker, R. J. , K. N. Erickson, R. L. Swanson, and J. R. Winckler, Substorm-associated particle boundary motion at synchronous orbit, *J. Geophys. Res.*, 81, 5541, (1976)

2. Russell, C. T., On the occurrence of magnetopause crossings at 6.6 Re, *Geophys. Res. Lett.*, 3, 593 (1976)

3. Studemann, W. B. Wilken, D. N. Baker, P. R. Higbie, R. D. Belian, and T. A. Fritz, *Planet. Space Sci.*, 34, 825 (1986)

4. Baker, D. N. Multipoint measurements of energetic particles in the magnetosphere, *Adv. Space Res.*, 8, #9, 385 (1988)

5. Baker, D. N., and R. L. McPherron, Extreme energetic particle decreases near geostationary orbit: A manifestation of current diversion within the inner plasma sheet, *J. Geophys. Res.*, 95, 6951-6599 (1990)

6. Baker, D. N., P. R. Higbie, E. W. Hones and R. D. Belian, High resolution energetic particle measurements at 6.6 Re, Low-energy electron anisotropies and short-term substorm predictions, *J. Geophys. Res.*, 83, 4863 (1978)

7. Korth, A., R. Friedel, D. N. Baker, H. Luhr, S. L. Ullaland, J. F. Fennell, and G. D. Reeves, Dynamics of the plasma sheet in the dawn sector of the magnetosphere: Observations from CRRES, to be published, *Proceedings of ICS-2* (1994).

8. Moldwin, M. B., M. F. Thomsen, S. J. Bame, D. J. McComas, J. Birn, G. D. Reeves, R. Nemzek and R. D. Belian, Flux Dropouts of Plasma and Energetic Particles at Geosynchronous Orbit During Large Geomagnetic Storms: Entry into the Lobes, submitted to *J. Geophys. Res.*, (1994)

9. M. H. Johnson and J. Kierein, Combined Release and Radiation Effects Satellite (CRRES): Spacecraft and Mission, *J. Spacecraft and Rockets*, 29, 556, (1992).

10. Vampola, A. L., J. V. Osborn, B. M. Johnson, CRRES Magnetic Electron Spectrometer AFGL-701-5A (MEA), *J. Spacecraft and Rockets*, 29, 592 (1992).

11. Wilken, B., W. Weiss, D. Hall, M. Grande, F. Soraas, J. F. Fennell, Magnetospheric Ion Composition Spectrometer Onboard the CRRES Spacecraft, *J. Spacecraft and Rockets*, 29, 585 (1992).

12. H. J. Singer, W. P. Sullivan, P. Anderson, F. Mozer, P. Harvey, J. Wygant, W. McNeil, Fluxgate Magnetometer Instrument on the CRRES, *J. Spacecraft and Rockets*, 29, 599 (1992).

13. Korth, A., G. Kremser, B. Wilken, W. Guttler, S. L. Ullaland, R. Koga, Electron and Proton Wide-Angle Spectrometer (EPAS) on the CRRES Spacecraft, *Journal of Spacecraft and Rockets*, 29, 609 (1992).

14. Hardy, D, Low Energy Plasma Analyzer (LEPA) on CRRES, *Nucl. Inst. and Methods*, 1993.

15. Kerns, K. J., D. A. Hardy, and M. S. Gussenhoven, Modeling of Convection Boundaries Seen by CRRES in 120-eV to 28 keV Particles, *J. Geophys. Res.*, 99, 2403, (1994).

16. Tsyganenko, N. A., Global Quantitative Models of the Geomagnetic Field in the Cislunar Magnetosphere for Different Disturbance Levels, *Planet. Space Sci.*, 35, 1347, (1987).

Eos, Transactions, American Geophysical Union, Vol. 77, No. 9, February 27, 1996, Pages 81, 86

GREAT DEBATES IN SPACE PHYSICS

The What, Where, When, and Why of Magnetospheric Substorm Triggers

Harlan E. Spence

Over the past three decades, terrestrial magnetospheric physics has had a unifying and hotly debated focus: the magnetospheric substorm. A magnetospheric substorm is a three-phase phenomenon [*McPherron*, 1979] in which energy is first extracted from the solar wind flow, transported, and stored within the Earth's magnetospheric magnetic fields (growth phase). The stored magnetic energy is then converted and released explosively within the magnetosphere and auroral ionosphere (expansion phase). Then the magnetosphere and auroral ionosphere relax, entering a quiescent state (recovery phase).

Understanding of this global process has unified the magnetospheric and auroral communities by providing the "big picture" of magnetospheric dynamics as a backdrop against which unrelated areas of more focused research may be put in context. The topic debated in the accompanying articles centers on one aspect of magnetospheric substorms, namely what triggers the expansion phase. The companion papers present two perspectives on substorm triggers: one advocates a trigger that is driven by an external change in the interplanetary magnetic field (IMF), while the other argues that external triggers are just one of many mechanisms that lead to the expansion phase, including internal instabilities.

What?

To appreciate the importance of the substorm "trigger," it is imperative to establish what a magnetospheric substorm is, at least phenomenologically. A consensus definition proposed many years ago stated that "A magnetospheric substorm is a transient process initiated on the night side of the Earth in which a significant amount of energy derived from the solar wind-magnetosphere interaction is deposited in the auroral ionosphere and magnetosphere" [*Rostoker et al.*, 1980]. The transient substorm effects are global, producing dramatic changes throughout geospace. These include major topological changes in magnetotail geometry as growth phase magnetic field stress is released, thermalization and bulk acceleration of magnetospheric particle populations both in the inner magnetosphere and the magnetotail as magnetic energy is converted to particle energy, and dramatic intensifications and motions of auroral emissions as electrical currents are driven in the auroral ionosphere.

The agreed upon definition above does not provide any physical explanation for what causes a magnetospheric substorm. A complete description requires a detailed explanation of how the solar wind flow couples energy into and through the magnetospheric system. Discussions of this subject have been the root of most contemporary debates in substorm physics. To keep study focused on what triggers the substorm, I avoid endorsing any one substorm model.

Two articles in this issue of *Eos* debate the following question: Are substorms triggered externally or internally? Lawrence Lyons, a scientist from The Aerospace Corporation, argues in favor of an external trigger while Anthony Lui, a scientist from the Johns Hopkins University Applied Physics Laboratory, argues for an internal trigger. Both authors present evidence to support their opposing views. To put their arguments in perspective, it is useful to first review the related body of work that precedes them.

If substorm onsets are triggered externally, phenomenological relationships between onsets and external boundary parameters should exist. Studies that investigated these factors were a thrust of early substorm research. Magnetospheric substorm strength (measured by the intensity of currents flowing in the ionosphere) was found to correlate strongly with the magnitude and sign of the north-south component of the interplanetary magnetic field (IMF). In most models, solar wind flow energy is imparted to the magnetosphere by way of dayside magnetic field merging between the southward component of the IMF carried past the Earth by the solar wind, and the northward directed geomagnetic field near the subsolar magnetopause boundary. In this picture, the coupled magnetosphere-ionosphere system is energized by its interaction with the solar wind/IMF. It is most highly energized when the IMF is most strongly southward. This strong control exerted by the IMF on substorm strength gave rise to the earlier related debate: Are substorm currents driven directly by the solar wind/IMF interaction (i.e., externally driven) or does the magnetosphere go through an energy loading-unloading process (which consists of external and possibly internal aspects)? As is the case in most "black-versus-white" arguments, subsequent studies demonstrated that the answer is "gray." Both driven and loading-unloading processes contribute to the magnitude of magnetospheric substorm currents.

Study next focused on whether the IMF controls not only the magnitude of substorms, but also directly triggers substorm onset. That brings us back to our main discussion. In June 1994, I cochaired a session devoted to substorm triggers with Terry Onsager of the NOAA/Space Environment Center at a National Science Foundation (NSF) Geospace Environment Modeling (GEM) Workshop in Snowmass, Colo. At this session, "Tail Geometry: IMF Control and Triggers," we asked Robert McPherron of UCLA to review studies from the 1970s and early 1980s that sought relationships between substorm expansion phase onsets and variations in the direction of the IMF (particularly northward excursions) or solar wind variations (for example, dynamic pressure changes discussed in Lui's article). McPherron reported a 45% likelihood that northward turnings of the IMF occur at the time of sharp substorm onsets, but that better determination of onset time and IMF data are needed. Workshop participants agreed that this was a topic that could be better quantified with both existing data sets and those to be obtained from upcoming solar-terrestrial missions. At this year's NSF/GEM summer workshop, Larry Lyons reported on a reinvestigation of the IMF-substorm connection. He made the strong assertion that "...most, and perhaps all, substorm expansion phases are triggered directly by IMF changes." This conclusion is the basis of his new view of substorms [*Lyons*, 1995]. That some or even many substorms are triggered by northward turnings is not controversial, but Lyons' statement that most or perhaps all fit this category, drew the attention of many people. Lyons recategorizes geomagnetic activity that lacks an IMF-induced trigger and that has previously been identified as a substorm to a different class of phenomenon. This reclassification yields his strong conclusion. That redefinition is a mat-

Boston University Center for Space Physics, 725 Commonwealth Avenue, Boston, MA 02215

0096/3941/7709/96/81/$01.00.

ter of ongoing debate and emphasizes the difficulty with semantics.

Tony Lui, who explains the other side of this debate, is an advocate of substorm trigger models based on plasma instabilities within the magnetosphere. In such models, a local instability occurs within the magnetosphere, perhaps as the result of global boundary conditions established by the solar wind/IMF. The internal instability however may occur without any variations in the IMF directly. Lui's article explores phenomenological evidence that supports the internal trigger hypothesis. Rather than searching for explicit signatures of an internal trigger, which may vary according to the chosen physical model, he seeks evidence for the absence of a consistent IMF variation associated with substorm onsets. Lui's review of the literature suggests that substorms can be triggered by a variety of external stimuli, but not exclusively by northward turnings of the IMF. This conclusion appears to be more widely accepted.

External and internal substorm trigger sources are entirely different scenarios that, in an ideal world, should be readily discernible and could be used to test the strengths of Lyons' and Lui's conclusions. Why, then, has this debate continued? The answer may in part be merely semantics. That aside, as we have learned in other fields of geophysics where nature is an uncontrolled "laboratory," for example, in earthquake prediction, that identifying a trigger mechanism is not always as straightforward as it appears. A shortage of possible physical theories is not the problem. Identifying trigger mechanisms is complicated by the available data. Imperfect observations are sometimes taken at the right times or places, or the correct measurements are obtained but at the wrong times or places. If we cannot determine trigger location and time well enough, any correlation with associated solar wind/IMF variations, which have their own measurement uncertainties, becomes problematic and leads to unclear answers. Uncertainties, then, in the "where" and "when" of the substorm trigger have limited our ability to reveal the "why."

Where?

One important aspect of the physics of the substorm trigger is the location where it operates. While the growth, expansion, and recovery phases all exhibit global behavior during substorms, it is not as clear where the expansion phase onset begins, initiating the global reconfiguration. Substorm phenomenology has very different "faces" depending upon where a particular measurement is made (that is, ground-based, ionosphere, geostationary orbit, or magnetotail) and what quantity is being measured (that is, magnetic or electric fields, charged particles, auroral luminosity, etc.). These factors influence the inferred onset location. Consequently, location estimates span a broad range, from near-geostationary orbit to the distant magnetotail to the auroral ionosphere. The size of the magnetosphere further confounds a simple resolution to this question. It is the largest of the geospheres with a volume of ~10^{31} cm^3. Spacecraft sample only a minute portion of this volume at any one time and, owing to the magnetosphere's dynamism, often cannot uniquely distinguish spatial from temporal variations. In spite of the enormity of the volume, the sparseness of data, and time dependence, heroic efforts have been made in our understanding of the magnetosphere and substorms. This is truly a triumph of space physics. Critical stages have included: establishing global auroral substorm phenomenology based on syntheses of local, ground-based observations [*Akasofu*, 1964]; quantifying magnetospheric boundaries and the different regions they delineate from exploratory spacecraft missions; and investigating the physics of individual magnetospheric regions using focused spacecraft missions. New capabilities provided through the coordinated, multipoint measurements of the International Solar Terrestrial Physics Program (ISTP) will allow us to advance our growing knowledge of substorm onset location.

When?

The question of where the trigger occurs is intertwined with the question of when signatures at various locations occur relative to one another. The magnetosphere-ionosphere system is electromagnetically coupled, so despite the great volume, substorm dynamics are evident across vast regions on relatively short timescales (seconds to minutes). As noted above, the differentiation of spatial and temporal variation is an inherently very difficult task, and especially so for substorm studies where strong spatial gradients and temporal evolution are both important. The question of when the various key phenomena occur at different locations and how they connect in a physical sense is therefore unresolved. High time resolution measurements throughout the critical active regions are still needed to establish what signature occurred first and therefore where the onset begins.

Why?

The "where" and "when" questions of substorm triggers outlined above speak to an uncertainty in our empirical view of substorms. These are needed before we can assuredly seek a clear association with possible external variations. Establishing these morphological characteristics are critical also for addressing the more fundamental physical questions of what the trigger mechanism is and why it operates at a given location and time in the substorm cycle. These underlying questions should become clearer as the phenomenology is clarified in the ISTP era. The substorm is one of the two most prominent dynamic responses of the terrestrial space physics environment to solar-induced variations (the other being magnetic storms) and is the most frequent one. Substorms are an important element of "space weather" and thus has not only a fundamental research motivation, but also a potentially practical application to space- and ground-based systems that may be vulnerable to variations of the natural space environment. By any measure, physical models are only as good as their ability to accurately predict a given phenomenon. At this stage, we do not understand the physics governing the substorm trigger well enough. This research area will undoubtedly yield the next generation of substorm models that go well beyond the ability to describe substorm phenomenology, but are truly predictive.

Acknowledgments

This work was supported by NASA under NAGW-3953. The format was motivated by the author's three young children, who have trained him to respond only to one-word queries.

References

Akasofu, S.-I., The development of the auroral substorm, *Planet. Space Sci., 12*, 273, 1964.

Lyons, L., A new theory of magnetospheric substorms, *J. Geophys. Res., 100*, 19,069, 1995.

McPherron, R. L., Magnetospheric substorms, *Rev. Geophys. Space Phys., 17*, 657, 1979.

Rostoker, G., S.-I. Akasofu, J. Foster, R. A. Greenwald, Y. Kamide, K. Kawasaki, A. T. Y. Lui, R. L. McPherron, and C. T. Russell, Magnetospheric substorms—definitions and signatures, *J. Geophys. Res., 85*, 1663, 1980.

J. Geomag. Geoelectr., **48**, 887 895, 1996

Low Altitude Signatures of the Plasma Sheet: Model Predictions of Local Time Dependence

Karen L. HIRSCH[1], Harlan E. SPENCE[1], and Terrance G. ONSAGER[2,3]

[1] *Center for Space Physics and Department of Astronomy, Boston University, Boston, Massachusetts, USA*
[2] *Space Science Center and Department of Physics, University of New Hampshire, Durham, New Hampshire, USA*
[3] *Now at NOAA Space Environment Center, Boulder, Colorado, USA*

(Received September 26, 1995; Revised March 19, 1996; Accepted April 15, 1996)

We combine two theoretical models of plasma sheet particle transport to trace plasma sheet particles from the nightside magnetospheric equatorial plane to low altitudes. We predict that the low-altitude signature of the plasma sheet is manifestly different at different local times. The Guiding Center Transport Model (GCTM) (Onsager *et al.*, 1993) uses a given particle energy, position, and an assumed magnetic and electric field to trace the low-altitude particle's trajectory to the plasma sheet. The Finite Tail Width Convection Model (FTWCM) (Spence and Kivelson, 1993) uses two Maxwellian plasma sources, one downtail and one on the dawnside boundary layer, to generate distribution functions across the tail plasma sheet. Using Liouville's theorem, the distribution functions at the equatorial level are projected to low altitudes. When this signature of the plasma sheet is projected to low altitudes near the Earth, the spatial variation in the equatorial plasma properties produce a latitudinal variation in the isoflux contours. Isoflux contours at high latitudes at dawn extend to lower latitudes at dusk, reflecting a larger plasma sheet plasma pressure at dusk than at dawn. This prediction is based solely on a projection of spatial variations in equatorial plasma properties.

1. Introduction

The macroscopic structure of the terrestrial plasma sheet is central to many large-scale aspects of magnetotail physics. For instance, in simple magnetohydrodynamic descriptions of the quasi-static tail, spatial gradients of the plasma sheet plasma pressure at the magnetic equatorial plane are a proxy for tail lobe magnetic field strengths (e.g., Spence *et al.*, 1989). Another example is time-dependent magnetotail convection models; the distributions of number density and pressure constrain magnetic-flux-tube volumes and hence magnetospheric convection (e.g., Erickson, 1992). In such descriptions of the plasma sheet, plasmas and magnetic fields are intimately linked and each provides unique yet coupled insights on the physics of the magnetotail.

Both theoretical models and empirical models may be used to describe the tail. Empirical models of the magnetic field in the magnetotail have improved steadily over the past two decades and are now used commonly as a research tool (Peredo *et al.*, 1993). Similar models of magnetotail plasmas are not in common use for several reasons: incomplete energy coverage of measured spectra; limited orbital coverage; and temporal/spatial ambiguity, since the transit time of a large apogee satellite is greater than the dynamic timescale, even during quiescent or quasi-static periods.

This last shortcoming is avoided at intermediate to low altitudes ($\lesssim 3\ R_E$), where polar orbiting spacecraft traverse the lower altitude extension of the plasma sheet (the so-called "horns") relatively quickly. These rapid passages yield "snapshots" of the equatorial plasma sheet. Studies have utilized this approach successfully (Suszcynsky *et al.*, 1993; Onsager and Mukai, 1995).

Despite the advantage gained by low altitude measurements of the plasma sheet, a single low-altitude spacecraft provides only one passage through the plasma sheet horns per orbit; and it occurs at only one fixed local time (equivalent to a single equatorial trajectory through the magnetotail plasma sheet). To construct an empirical two-dimensional, instantaneous map of plasmas in the equatorial plane requires many satellites traversing the plasma sheet horns simultaneously at various local times. Such multi-satellite studies have not been available routinely.

In this paper, we complement single spacecraft low-altitude data studies. We combine two published theoretical models of magnetospheric particle transport to predict the low-altitude signature of the plasma sheet as a function of local time. One model specifies the plasma thermal pressure and density throughout the equatorial magnetotail. The other specifies the mapping of plasma properties between the equatorial plane and intermediate altitudes. The magnetotail plasma model is quasi-static yet predicts spatial gradients of the macroscopic plasma quantities. These cross- and down-tail variations at the equatorial plane produce differences in the low-altitude plasma sheet signatures at different local times. It is important to stress that the predicted local time differences arise from spatial differences, a conclusion not easily reached from a single spacecraft passage through the plasma sheet horns. We suggest that model syntheses of this type improve the interpretation of low-altitude plasma sheet signatures.

2. Models

2.1 Guiding center transport model

The Guiding Center Transport Model (Onsager *et al.*, 1993) traces guiding centers of ions and electrons between low altitudes and the magnetic equatorial plane. The particle guiding centers are traced backwards in time to determine the source locations in the equatorial plane of particles detectable by a low-altitude spacecraft. For the purposes of this research, we have considered only protons. Protons are followed as they travel through specified electric and magnetic fields; their energy and magnetic moments are conserved as their guiding centers are traced. The electric field is an imposed dawn to dusk field across the tail; magnetic field lines are assumed to be equipotentials. The magnetic field model used is the Tsyganenko model (Tsyganenko, 1987). The magnetic field model is parameterized by the K_P index and the dipole tilt angle.

In Fig. 1, we show a typical guiding center trace in the X_{GSM}-Z_{GSM} plane. The dashed line is the trace of the guiding center. The solid lines are the magnetic field lines. The particle's guiding center trajectory in two dimensions is determined by the integral effects of its $\mathbf{E} \times \mathbf{B}$ drift velocity across magnetic field lines and its velocity along the magnetic field lines. The particle being traced "backwards" from an altitude of 10,000 km and at ~73° magnetic latitude is a 2 keV proton with a 10° pitch angle. These specify the initial velocity components and following the guiding center to its origin, we find that this particle originated in the plasma sheet at $X_{GSM} = -53\ R_E$. In this example of how the GCTM maps guiding centers, the dipole tilt angle was −29° and the $K_P = 3$.

The inputs to the GCTM are the position, pitch angle (here assumed to be 10°), and energy of the particles detectable at low altitudes. The positions are chosen to represent a polar orbiting satellite trajectory at several fixed magnetic local times. For the results described here, we have assumed an electric field that corresponds to an $\mathbf{E} \times \mathbf{B}$ drift speed of 1 km/s equatorward at the initial low altitude position (~10,000 km). This electric field when mapped along the assumed equipotential magnetic field to the equatorial plane yields an electric field of about 0.08 mV/m at $X_{GSM} = -60\ R_E$ and about 0.15 mV/m at $X_{GSM} = -15\ R_E$. These values of the electric field correspond to earthward convection speeds in the plasma sheet of about 50 km/sec at $X_{GSM} = -60\ R_E$ and about 25 km/sec at $X_{GSM} = -15\ R_E$. The inputs to the magnetic field model are the dipole tilt angle and the K_P used for Fig. 1.

The model specifies the particle's position in the equatorial plane and its energy, but not its

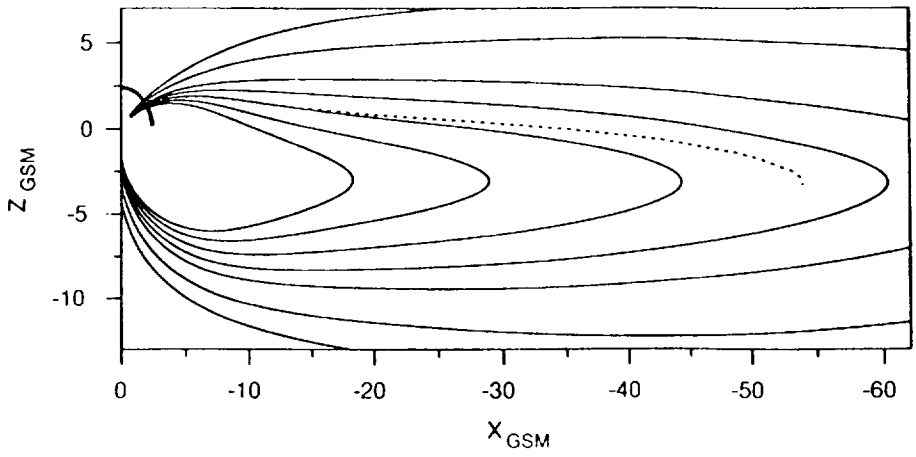

Fig. 1. A cartoon of the Guiding Center Transport Model. The dashed line represents a 2 keV proton originating in the plasma sheet at $X = -53\ R_E$ detected at ~10,000 km in altitude at 73° latitude. The $K_p = 3$; the Earth's dipole is tilted −29°.

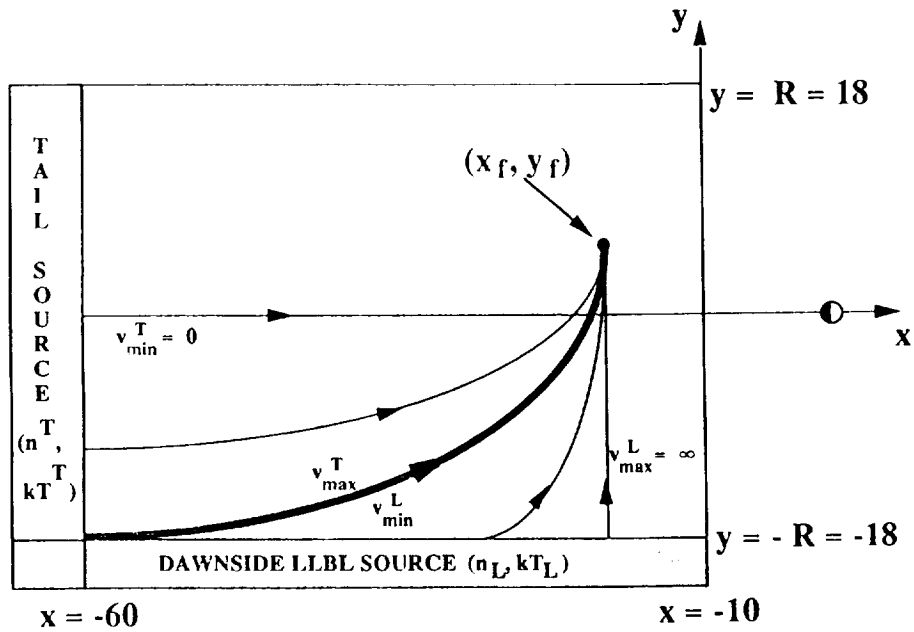

Fig. 2. A cartoon of the Finite Tail Width Convection Model. There are two sources of plasma, both Maxwellian: the dawnside low-latitude boundary layer and the tail source. Particles drift from the source regions and the two sets of particles at a given point are then summed (Spence and Kivelson, 1993).

flux. To determine the proton flux we must know the phase space density at the equatorial plane. The plasma conditions throughout the plasma sheet equatorial plane have been calculated using the Finite Tail Width Convection Model (FTWCM) (Spence and Kivelson, 1993) (hereinafter referred to as SK93).

2.2 The finite tail width convection model

The FTWCM is a bounce averaged drift model for ions. It describes the bulk plasma properties in the magnetotail from $-10 \leq X_{GSM} \leq -20$ and $|Y_{GSM}| \leq 20\ R_E$ at the magnetic equator. This model has been described extensively elsewhere (Kivelson and Spence, 1988; Spence and Kivelson, 1990, and SK93) and is summarized only briefly here.

The model has two sources of particles which populate the plasma sheet: the low-latitude boundary layer and the distant magnetotail. Figure 2 is a cartoon depicting the model and its sources. The model has five input parameters: proton number density and temperature for both plasma sources and the cross-tail electrostatic potential. Both plasma source distributions are assumed isotropic and Maxwellian. An additional parameter that the model requires is the flux-tube volume along the midnight meridian. This is calculated using the Tsyganenko 1987 long model (Tsyganenko, 1987).

Particles drift both earthward and from dawn-to-dusk under the influence of $\mathbf{E} \times \mathbf{B}$ and $\nabla \mathbf{B}$ drifts from the source distributions. For a finite width tail, only those protons starting in the deep tail (dawn boundary layer) with velocities less (greater) than some limiting velocity can reach any given final position. At this final location, the ensemble distribution function is the sum of those portions of the source distributions that can gain access. The plasma moments have finite velocity limits and this modifies densities and pressures as a function of position within the tail.

Figure 3 illustrates the model outputs: plasma density and thermal pressure calculated as a function of position in the magnetic equatorial plane. For our study, representative quiet magnetospheric conditions were used. The model inputs are as follows: a cross tail potential of 15 kV; a far-tail plasma source temperature, $kT_T = 2.5$ keV and number density, $n_T = 0.1$ cm^{-3}; and a low-latitude boundary layer temperature, $kT_L = 0.7$ keV and number density, $n_L = 0.5$ cm^{-3}. These values are identical to those motivated by and used in SK93. The top panel of Fig. 3 shows number density contours in number/cm^3 plotted in the equatorial plane, where the vertical axis is Y_{GSM} and the horizontal axis is X_{GSM}. The middle panel shows thermal pressure in nDynes/cm^2. The bottom panel shows the temperature contours in keV.

Note that each panel demonstrates the strong x-dependent variation owing to adiabatic compression as well as a y-dependent variation owing to gradient drift effects. The earthward increases in density and pressure are well studied and understood in terms of convective transport and stress balance (Lui *et al.*, 1994; Spence *et al.*, 1989). The crosstail variation has been less studied empirically and warrants discussion in the context of this paper.

The large crosstail plasma pressure gradient must be in stress balance with the coincident magnetic geometry in the magnetostatic limit. This is not true for the FTWCM using the Tsyganenko 1987 long model, as the magnetic field was not self-consistently readjusted according to the predicted plasma pressures. Nevertheless, we believe that the FTWCM provides a reasonable first-order approximation. For example, the model cross-tail pressure gradient was considered by SK93. They reasoned that pressure balance cannot be maintained by an equal and opposite crosstail lobe magnetic pressure gradient. Instead, they proposed a magnetic pressure gradient within the plasma sheet which increases from dusk to dawn. Evidence for this condition was found not only in tail plasma sheet plasma pressure surveys (Liu and Rostoker, 1991), but also in magnetic surveys (Fairfield, 1986). The empirical models compare favorably with the FTWCM model results (see SK93). We appeal to this explanation for consideration of the appearance of this cross- (and down-) tail variation at low altitudes.

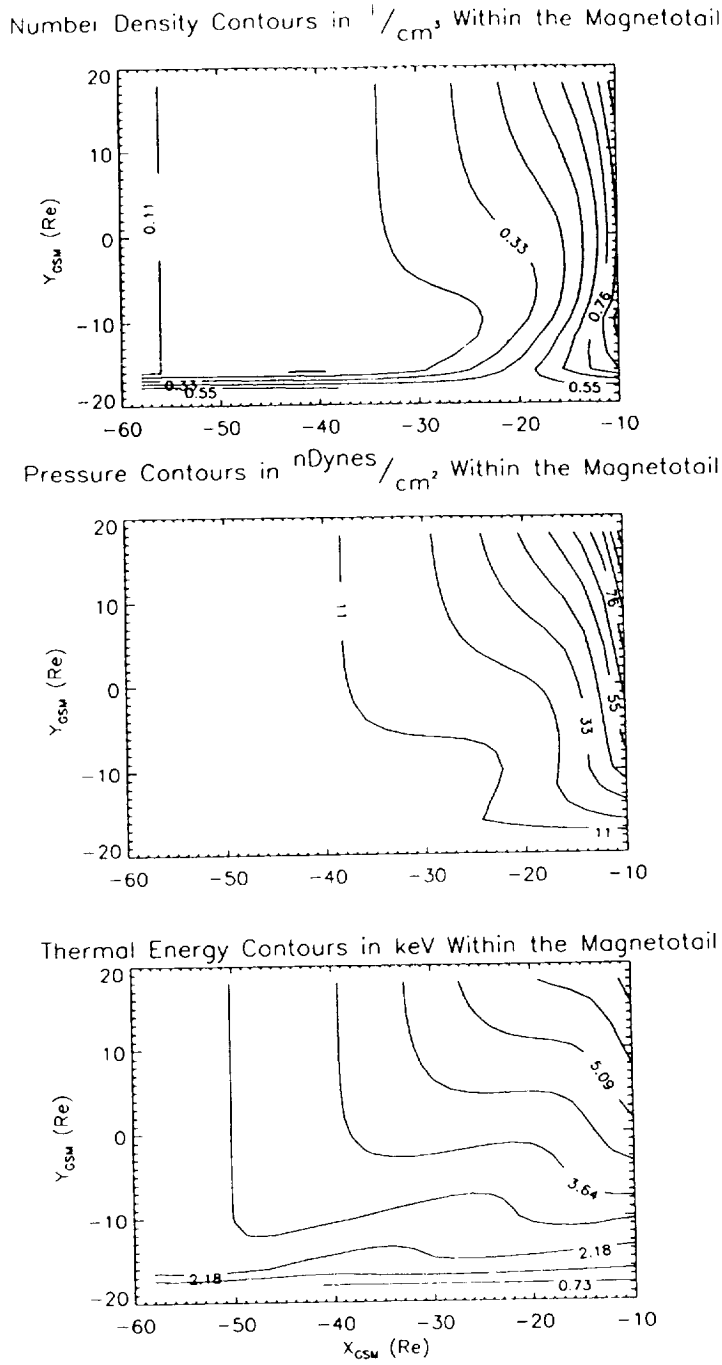

Fig. 3. Contours within the plasma sheet. These contours were generated using the finite tail width convection model. The top panel consists of number density contours across the tail; the middle is thermal pressure contours; and the bottom panel is thermal energy contours.

3. The Melding of the Models

The GCTM output gives a position and an energy in the near-tail equatorial plane corresponding to the source location of a particle detected along the low-altitude spacecraft trajectory. At these positions, the FTWCM can then be used to determine the distribution function as a function of energy. Using Liouville's theorem, the values of phase space densities in the equatorial plane can be assigned to the corresponding locations at low altitudes for comparison with a polar orbiting spacecraft, such as Akebono. Such comparisons have been made recently by Onsager and Mukai (1995). In their work, they arbitrarily specified phase space densities at the equatorial plane and restricted their attention to one magnetic meridian (local time) at low altitudes. In this paper, we extend their approach by investigating the low-altitude plasma sheet signature at several local times in the context of a two-dimensional physically-motivated model of plasma at the equator.

In combining the models, the assumptions and inputs are as consistent as possible. For example, the magnetic field model used is the same for both models. Other aspects of the models differ slightly in approach but these differences do not affect the results of the mappings qualitatively. For example, the electric fields are treated somewhat differently in each model. The electric field magnitudes at the equatorial plane are similar at the down-tail boundary of the FTWCM, but differ by a factor of two at the earthward boundary. We stress that for the GCTM results presented here, the calculated low-altitude spectra are governed primarily by the magnetic field mapping between the low-altitude locations and the plasma sheet. In these cases, the details of how the electric field is distributed are a secondary effect and are not treated in this study.

To illustrate the model synthesis we chose to generate synthetic spectra that a low-altitude spacecraft plasma analyzer (such as on the Akebono spacecraft (Mukai *et al.*, 1990)) would be able to observe. We chose Akebono because it has been used recently in such studies (Onsager and Mukai, 1995). Accordingly, the energy bins used for the GCTM were chosen to match Akebono energy bins and initial low-altitude locations were chosen along orbital tracks of a polar orbiting spacecraft at three local times. The FTWCM parameters were chosen to match the SK93 values. The synthesized model results are thus representative of relatively quiet magnetospheric conditions. The results shown in Fig. 4 demonstrate the prediction of the plasma sheet's projection to various low-altitude locations in a general sense. Of course, any comparison of the model with real data would require selection of model parameters consistent with actual conditions.

Figure 4 shows the combined model output of spectra that we predict would be measured by three spacecraft simultaneously traversing the "horns" at three local times: ~2200 hours, midnight, and ~0200 hours. The vertical axis is energy measured on a logarithmic scale. The horizontal axis is magnetic latitude. The contours are differential energy flux. White on this scale represents flux levels below the simulated detector threshold here consistent with the Akebono Low Energy Particle (LEP) sensors.

Figure 4 describes the predicted signature of the plasma sheet at low altitudes as a function of local time. This figure illustrates that low-altitude data can be used to remotely sense plasma sheet conditions. For example, at any particular local time pass, the flux intensity increases as the spacecraft moves to lower latitude reflecting the earthward compression of plasma and the commensurate rise in number density. Also, the energy width of the flux contours increases equatorward, reflecting the earthward increase of plasma sheet pressure and temperature. The flux levels can be used quantitatively to infer plasma sheet bulk properties.

Of more interest for this paper, though, are the predicted local time dependences which also mirror plasma sheet conditions. The important feature on these plots is the apparent latitudinal position of the outer edge of the plasma sheet signature (identified by the first observable isoflux level) at the three local times. The y-dependence of the plasma sheet temperature (see bottom

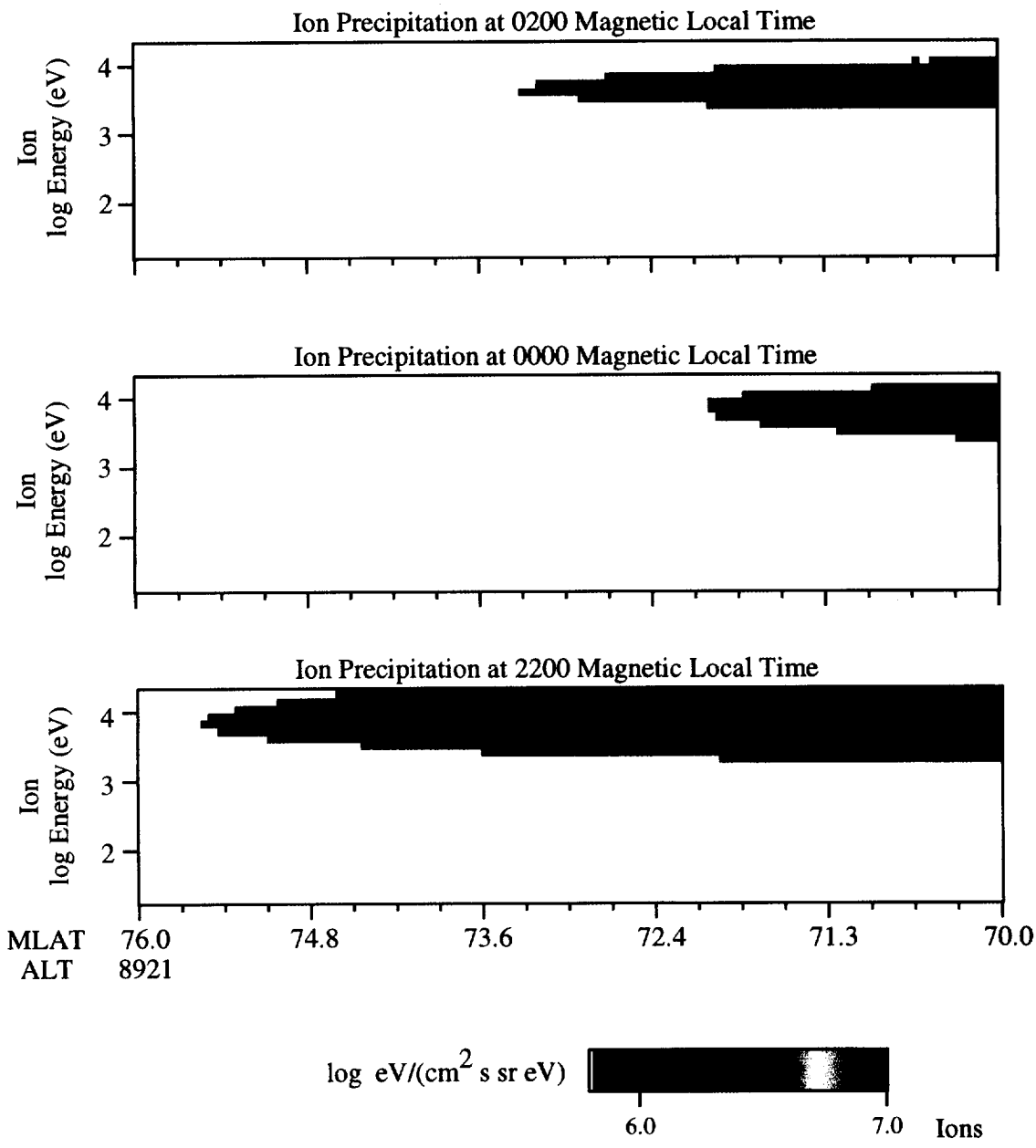

Fig. 4. The model output compared at three local times: midnight, 0200, and 2200. White represents differential energy fluxes below the threshold.

panel of Fig. 4) yields a clear local time dependence at low altitudes: the flux energy width (a measure of temperature) increases from the top to bottom panel of Fig. 4, consistent with the dawn-to-dusk energy gradient. This is most clearly seen when comparing the profiles at 2200 and 0200 magnetic local time where the magnetic mappings, which affect the latitudinal appearance of the plasma sheet, are identical within the symmetric Tsyganenko model. The mapping of the

Tsyganenko model also explains why the midnight mapping of the first isoflux contour is at lower latitudes, since the field is more stretched near midnight.

4. Conclusions

Two models were linked: the finite tail width convection model and the guiding center transport model. Their output makes specific predictions for plasma sheet ion fluxes detectable at low-altitudes. Specifically, before local midnight, the plasma sheet appears to be hotter and the particle isofluxes are visible at higher invariant latitudes than after local midnight.

The spectra in Fig. 4 show the spatial variations in the plasma sheet signature; the invariant latitude where the protons have the same flux differ with local time as does the energy width of the measured flux. The importance of this model is that it is time-independent. Therefore, all model predictions for differences in the plasma sheet signature are due to spatial effects: the projection to low altitudes of the plasma pressure asymmetry in the equatorial plane. This asymmetry is due to the differential drift of plasma across the tail. This type of variation should be readily apparent in concurrent satellite passes at low or middle altitudes at several local times.

These models can be used to compare near-simultaneous measurements by multiple spacecraft. Currently we are in the process of assessing the models against ISEE-2 data (Hirsch *et al.*, 1995). The ideal test case is simultaneous measurements at different local times from two or more spacecraft. During the International Solar-Terrestrial Physics program it is of great importance to have diagnostic tools such as this one to develop links between low and middle altitude crossings of the plasma sheet horns and the equatorial plane.

This work was supported by a Presidential University Graduate Fellowship from Boston University (KLH); under the NASA grant NAGW-3953 and NSF grant ATM-9458424(HES); and under the NASA Supporting Research Technology grant NAGW-2505 and NSF grant ATM-93008322 (TGO).

REFERENCES

Erickson, G. M., A quasi-static magnetospheric convection model in two dimensions, *J. Geophys. Res.*, **97**, 6505 6522, 1992.

Fairfield, D. H., The magnetic field of the equatorial magnetotail from 10 to 40 R_E, *J. Geophys. Res.*, **91**, 4238 4244, 1986.

Hirsch, K. L., H. E. Spence, T. G. Onsager, and M. F. Thomsen, A case study of the local-time dependence at mid-altitudes of the plasma sheet, *AGU Fall 1995, EOS Transactions*, **76**, 46, 1995.

Kivelson, M. G. and H. E. Spence, On the possibility of quasistatic convection in the quiet magnetotail, *Geophys. Res. Lett.*, **15**, 1541 1544, 1988.

Liu, W. W. and G. Rostoker, Effects of dawn dusk pressure asymmetry on convection in the central plasma sheet, *J. Geophys. Res.*, **96**, 11,501 11,512, 1991.

Lui, A. T. Y., H. E. Spence, and D. P. Stern, Empirical modeling of the quiet time nightside magnetosphere, *J. Geophys. Res.*, **99**, 151–157, 1994.

Mukai, T., N. Kaya, E. Sagawa, M. Hirahara, W. Miyake, T. Obara, H. Miyaoka, S. Machida, H. Yamagishi, M. Ejiri, H. Matsumoto, and T. Itoh, Low energy charged particle observations in the "auroral" magnetosphere: first results from the Akebono (EXOS-D) satellite, *J. Geomag. Geoelectr.*, **42**, 479 496, 1990.

Onsager, T. G. and T. Mukai, Low altitude signature of the plasma sheet boundary layer: observations and model, *Geophys. Res. Lett.*, **22**, 855–858, 1995.

Onsager, T. G., C. A. Kletzing, J. B. Austin, and H. MacKiernan, Model of magnetosheath plasma in the magnetosphere: Cusp and mantle particles at low altitudes, *Geophys. Res. Lett.*, **20**, 479, 1993.

Peredo, M., D. P. Stern, and N. A. Tsyganenko, Are existing magnetospheric models excessively stretched?, *J. Geophys. Res.*, **98**, 15,343 15,354, 1993.

Spence, H. E. and M. G. Kivelson, The variation of the plasma sheet polytropic index along the midnight meridian in a finite width magnetotail, *Geophys. Res. Lett.*, **17**, 591 594, 1990.

Spence, H. E. and M. G. Kivelson, Contributions of the low-latitude boundary layer to the finite width magnetotail convection model, *J. Geophys. Res.*, **98**, 15,487–15,496, 1993.

Spence, H. E., M. G. Kivelson, R. J. Walker, and D. J. McComas, Magnetospheric plasma pressures in the midnight meridian: observations from 2.5 to 35 R_E, *J. Geophys. Res.*, **94**, 5264 5272, 1989.

Suszcynsky, D. M., J. T. Gosling, and M. F. Thomsen, Ion temperature profiles in the horns of the plasma sheet, *J. Geophys. Res.*, **98**, 257–262, 1993.

Tsyganenko, N. A., Global quantitative models of the geomagnetic field in the cislunar magnetosphere for different disturbance levels, *Planet. Space Sci.*, **35**, 1347–1358, 1987.